5-2016

EFFECT OF SURFACTANT ON STRUCTURAL AND ELECTROCHEMICAL PROPERTIES OF NICKEL OXIDE

Muidh Albalawi
Pittsburg State University

EFFECT OF SURFACTANT ON STRUCTURAL AND ELECTROCHEMICAL PROPERTIES OF NICKEL OXIDE

A Thesis Submitted to the Graduate School
in Partial Fulfillment of the Requirements
for the Degree of
Master of Science

Muidh Albalawi

Pittsburg State University

Pittsburg, Kansas

May, 2016

EFFECT OF SURFACTANT ON STRUCTURAL AND ELECTROCHEMICAL PROPERTIES OF NICKEL OXIDE

Muidh Albalawi

APPROVED:

Thesis Advisor _____
Dr. Ram Gupta, Department of Chemistry

Committee Member _____
Dr. Pawan Kahol, Department of Physics

Committee Member _____
Dr. Khamis Siam, Department of Chemistry

Committee Member _____
Dr. John Franklin, Department of English and Modern Languages

Acknowledgements

I would like to thank my lovely mother for all her prayers and support. I am grateful to my wonderful wife, Manal. She stood beside me, supporting and driving me toward achieving my goals and what's more than this, she was sharing with me through the good times and bad. Also, I would like thank my son, Yamin, may God grant me children as good as my son. And, I would like to thank my brothers and sisters.

Actually, my words are powerless to express my gratitude to my adviser Dr. Ram Gupta. I want to deeply say thank you to him for his guidance and recommendations which allowed this work to be completed. I appreciate his patience and his advice and the effort he undertook to teach me and improve my skills. This work would not have been completer were it not for his contributions and suggestions.

In addition, I would like to express the deepest appreciation to all my committee members: Dr. John Franklin, Dr. Pawan Kahol, and Dr. Khamis Siam. Also, I would like to thank Dr. Lifeng Dong from Missouri State University for his assistance in recording SEM images of my samples.

Finally, I would like to thank the Department of Chemistry at Pittsburg State University and my patron Saudi Food and Drug Authority for allowing me to further my knowledge.

EFFECT OF SURFACTANT ON STRUCTURAL AND ELECTROCHEMICAL PROPERTIES OF NICKEL OXIDE

An Abstract of the Thesis by
Muidh Albalawi

Today, the increasing demand for energy in the world has led to a focus on efficient and low cost energy storage devices. Many essential energy sources take a significant number of forms, including atomic energy and conventional sources, such as petroleum, coal and natural gas. Recently, supercapacitors have attracted research due to their high power densities, quick charge-discharge and long life cycles. The objective of this thesis is to alter the morphological structure of nickel oxide (NiO) utilizing different surfactants and furthermore to analyze the impact of these surfactants on the electrochemical properties of the nickel oxide. The unlimited applications of nickel oxide relate to lower cost, commercial availability and high electrochemical properties. The nickel oxide was synthesized by a hydrothermal method. For the amalgamation of nickel oxide for changing morphologies, nickel (II) nitrate hexahydrate, urea $CO(NH_2)_2$, ammonium fluoride (NH_4F), cetyltrimethylammonium bromide (CTAB), poly (vinyl pyrrolidone) (PVP), sodium dodecyl sulfate (SDS) were used for the synthesis nickel oxide. The obtained precursor was calcined at 500 °C to prepare phase pure nickel oxide. The crystal size determined using XRD for NiO-SDS was observed to be 27.5 nm. The electrochemical properties of the nickel oxide were studied using cyclic voltammetry and galvanostatic charge –discharge measurements. The highest specific capacitance of 315 F/g was observed in 3 M LiOH for NiO-SDS sample at scan rate of 5 mV/s.

TABLE OF CONTENTS

CHAPTER **PAGE**

LIST OF TABLES

TABLE **PAGE**

LIST OF FIGURES

FIGURE **PAGE**

CHAPTER I

INTRODUCTION

Today, increasing population leads to higher demand for energy in the world. There are many essential energy sources that take a significant number of forms, including atomic energy and conventional sources. Some of the most popular conventional sources are petroleum, coal and natural gas (See Table 1.1).

Table 1.1: Total world electricity generation by energy source in 1971 and 2009(1)

1971		2009
Power Source	Electricity Generation (TWh)	Electricity Generation (TWh)
Coal and Peat	2102	8119
Oil	1097	1027
Natural Gas	695	4230
Nuclear	111	2697
Hydro	1203	3252
Other/renewables	36	660

There are other energy resources which are renewable in nature such as wind, sun and hydropower. The energy produced from these resources is called green energy. Significant efforts have been paid in utilizing these renewable resources for energy. Table

1.2 compares the power produced using wind energy. As seen, a significant amount of energy is being generated using wind and has continued to increase in recent years (1).

Table 1.2: Comparable wind power capacity (MW) between 2010 and 2015 in U.S state (2).

State	Wind Power capacity2010	Wind Power capacity2015
Kansas	1074	3,766
Missouri	457	459
Nebraska	213	890
Colorado	1299	2,992
Texas	10,089	17,713
Iowa	3675	6,212
Oklahoma	1482	5,148
California	3253	6,108

The wind energy is generated by transferring wind flow to electrical force through air turbines. This energy, which was produced by wind turbines, can be wasted if there is no efficient storage. There are a lot of techniques that can be used to store wind energy. Pumped –storage hydroelectricity is one of the kinds of storage of wind energy and hydro-energy. The concept of this technique depends on the gravitational potential of water by pumping from lower pond storage to higher pond storage using wind turbines or solar energy (3).

Solar energy is one of the most popular sources for green energy production. On average, each day the earth receives about 1.2×10^{5} TW energy from the sun (4). The sun

generates its vitality by the nuclear reaction of hydrogen to helium. Sunlight may be that principle wellspring for vitality of the surface of the earth. The biomaterials utilize the sun energy through photosynthesis reaction to provide food and energy. The plants capture the solar energy and change it to chemical form (5). Solar cells are popular devices which transfer the sunlight into electricity using appropriate materials. Solar cell technologies are traditionally divided into three generations (6). The first generation utilized silicon wafers to fabricate solar cells. These solar devices showed an efficiency of about 20%. The second generation for solar cells was based on amorphous silicon, copper indium gallium di-selenide (CLGS) and cadmium tellium. The materials used in the second generation were cheaper in cost because they did not utilize silicon wafers. The third generation of solar cells is based on thin layers of organic materials or polymers. This kind of solar cell has big advantages compared to other solar cell devices including simplicity, easy fabrication, and lower cost. The biggest advantage of this generation of solar cell is that it uses materials that are readily available and their properties can be tuned by simple chemical modifications. A hydropower is another way to generate electricity by the motion of water (kinetic energy). Those kinds of energy sources have taken an important place during the last few years.

1.1: Energy Storage Devices

Regardless of the methods used to generate green energy, we have compelling reasons to store this created energy efficiently and with the goal that it might be utilized later as per our need. Batteries, fuel cells and capacitors are some of the widely used energy storage devices. Each device has its own advantages and disadvantages. The energy storage capacity such as energy density and power density depends on the type of

device used. A comparison of the power energy densities of these devices is shown in Figure 1.1.

Batteries are devices which generate electricity by chemical reaction. The famous electrical batteries in this section are galvanic cell or voltaic cell, an electrochemical cell that gives electrical power by redox reaction occurring inside the cell as shown in Figure 1.2. Lead acid batteries have been utilized for more than 130 years and they are still the most widely used batteries due to their advantages. For example, in China this battery is used to generate around 75% of the energy. Nickel- cadmium batteries are a close second to lead acid batteries in the market. They have longer life and higher density power when compared with lead acid batteries.

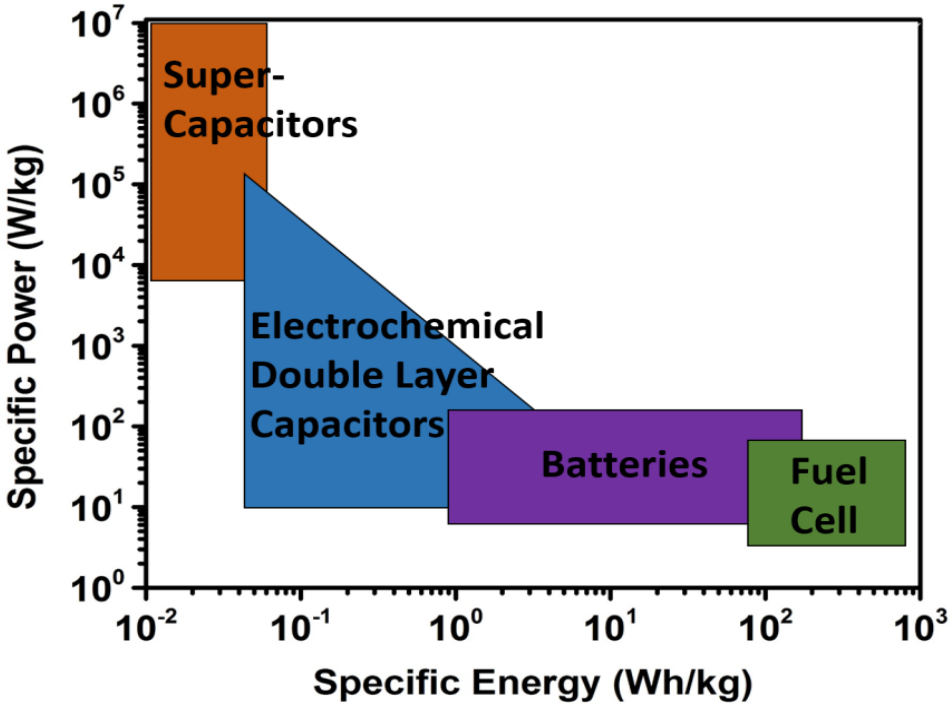

Figure 1.1: Ragone plot for various kinds of energy storage devices (7).

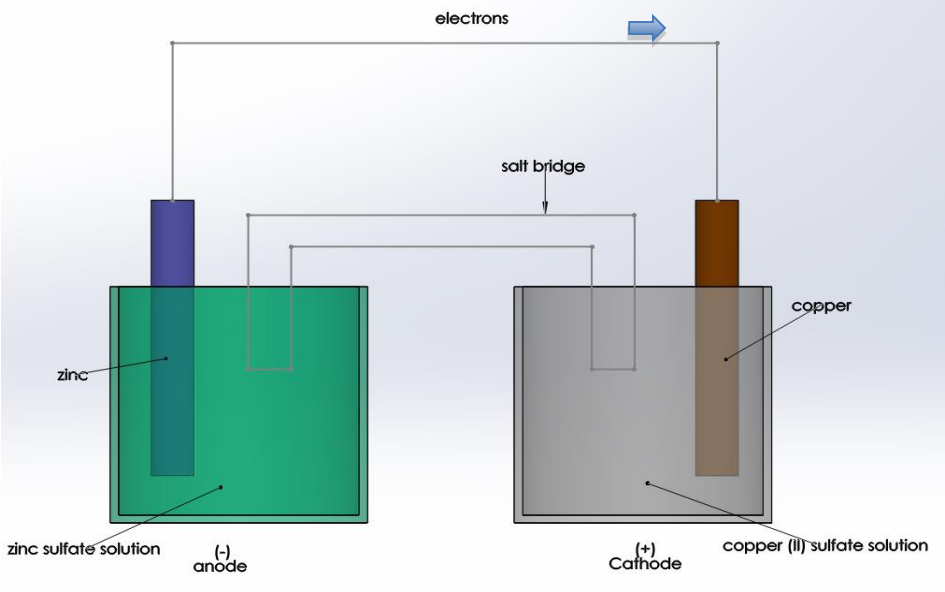

Figure 1.2: Schematic diagram of a galvanic cell.

Other types of batteries such as sodium sulfur batteries have attracted considerable attention in recent years due to their higher storage capacity (~305 MW) (3). Due to the chemical reaction involved in these batteries, their performance and life is limited. They use chemicals which are toxic in nature, creating environmental concerns. The second most popular energy storage devices are capacitors. A capacitor is energy storage device that stores energy due to electrostatic or Faradaic reactions. The most common form of a capacitor is the electrochemical double layer capacitors which utilizes parallel plates to store energy. The schematic of an electrochemical double layer capacitor is shown in Figure 1.3.

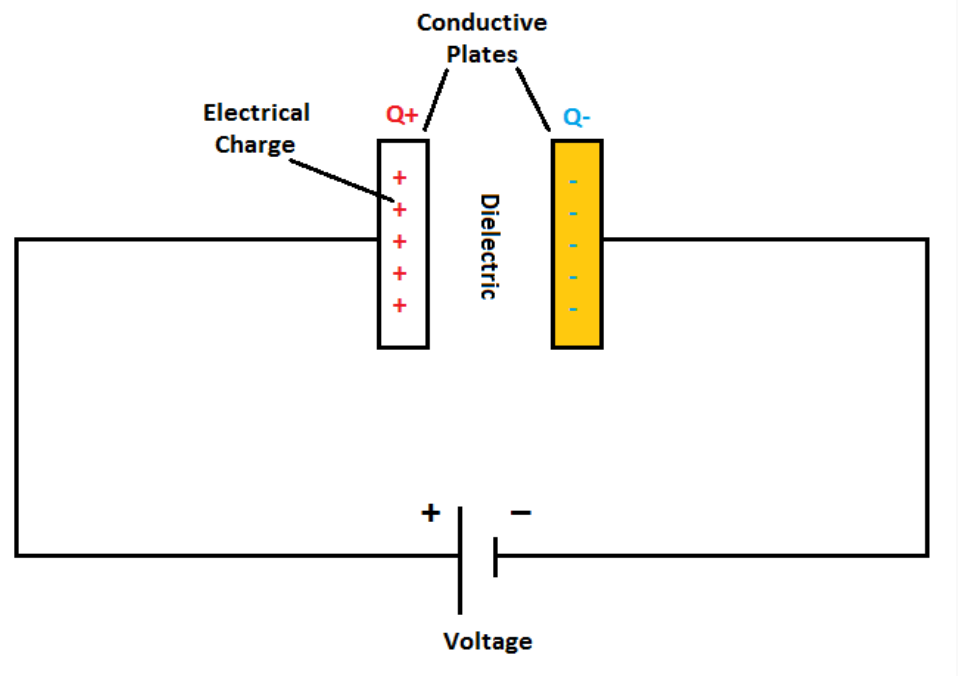

Figure 1.3: Schematic capacitor construction.

In such devices, when voltage (V) is applied, the cell gets an electrical field in the dielectric plate and the electrical field will cause separation of a positive charge (+Q) on one side of the capacitor and a negative charge (-Q) on the other. The capacitance of such a device can be measured by (8):

$$C = Q/V \quad \text{..... (1),}$$

where V is the applied voltage and Q is the charge.

The charge storage capacity of these capacitors can be improved by utilizing nanostructured metal oxides or highly porous carbon. Such high capacity devices are called supercapacitors or ultracapacitors. Supercapacitors provide higher charge storage capacity and better performance compared to conventional capacitors. Supercapacitors are mainly divided into three categories based on their charge storage mechanism which is shown in Figure 1.4 (9).The first one is called electrical double-layer capacitors

(EDLC) where a charge is stored based on the separation of positive and negative charges at their respective plats. The electricity may be a physical charge detachment that is saved at those interfaces between the electrodes and the electrolytes. It communally uses carbon and graphite as electrodes for charge storage.

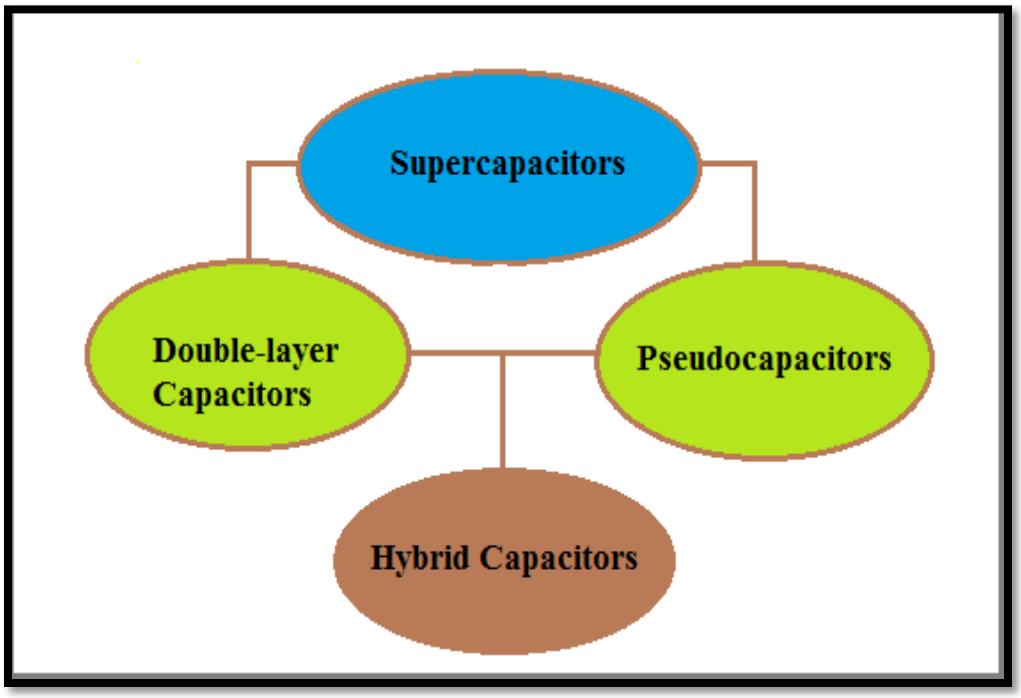

Figure 1.4: Types of supercapacitors.

The performance of an electrical double layer capacitor can be improved by utilizing electrode with higher surface area (Figure 1.5). The charge storage capacity of an electrode is directly proportional to its surface area by the equation given below:

$$C = \frac{\varepsilon A}{d} \quad \text{.....(2),}$$

where ε is the dielectric constant, A is the electrode surface area and d is the distance between the electrodes. This suggests that utilizing a material with higher surface area could provide a device with a higher charge storage capacity. The charge storage capacity

and energy of the device depends on the voltage. The relationship between energy and voltage is given below (8):

Energy, $W = \frac{1}{2}CV^2$ in Joules (j)..... (3),

where C (F/g) is specific capacitance and V (V) is the potential window.

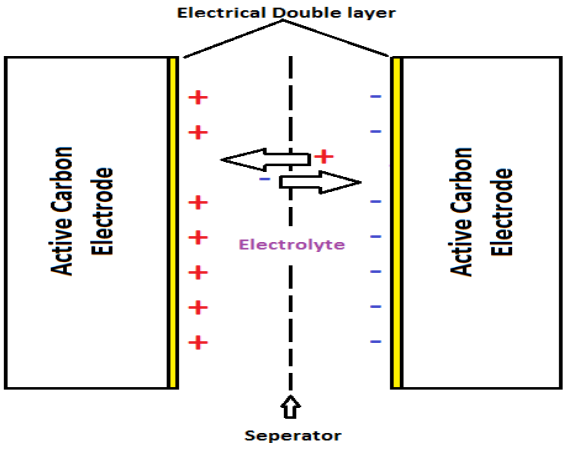

Figure 1.5: Schematic electrical double layer.

As seen in the equation 3, voltage plays a vital role in energy storage capacity. Aqueous electrolytes have limitations about the voltage as a maximum of 1V could be applied. Higher voltage will lead to the electrolysis of water. The performance and capacity of a device could be improved by utilizing non-aqueous electrolytes. So, if electrolytes change to organic, the energy density will be increased as now we can apply higher voltage (around 2.7 V). The second type of capacitor is pseudocapacitors. In pseudocapacitors, Faradaic charges are transferred between electrode and electrolyte by reduction-oxidation reactions and intercalation processes. The most commonly used materials for such kind of capacitors are metal oxides and conducting polymers.

Ruthenium oxide is an example of a metal oxide that can provide higher charge storage capacity.

A hybrid capacitor combines the properties of both electrical double-layer capacitors and pseudocapacitors and thus provides higher charge storage capacity (10).

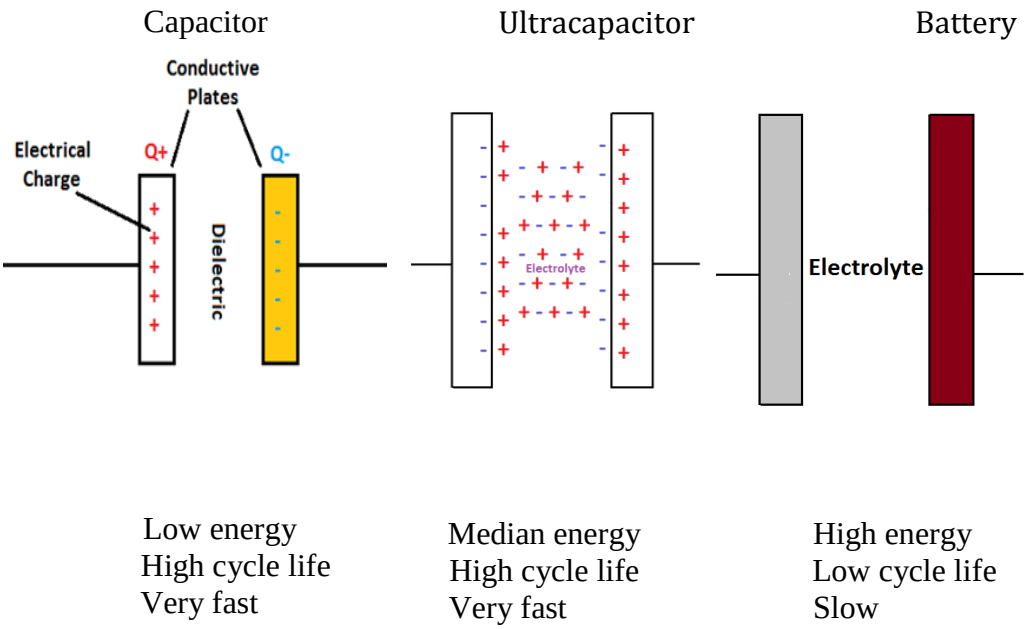

Figure 1.6: Comparison between capacitor, ultracapacitor and battery.

1.2: Project Rationale

The electrochemical properties of the metal oxides and their charge storage capacities rely on their size, morphology and porosity. The properties of metal oxides might be tuned toward developing a high performance capacitor by modifying their morphologies and surface area. The primary objective for this thesis is to alter the morphological structure of the nickel oxides utilizing different surfactants and to analyze the impact of such changes on their electrochemical properties. Nickel oxides have several advantages such as lower cost, commercial availability and higher electrochemical performance compared to other metal oxides. There are several ways to synthesize NiO nanoparticle such as thermal decomposition, sol-gel and hydrothermal (11). Liu and Anderson studied electrochemical proprieties of nickel oxide and reported that a very high specific capacitance (~ 2573 F/g) can be achieved theoretically (12). Leontyeva et al. have synthesized nanocomposites of NiO with carbon and observed good electrochemical performance of the composite (13). These composites showed a specific capacitance of 1100 F/g and 750 F/g based on cyclic voltammetry and charge – discharge measurements, respectively. Justin et al. have synthesized NiO under three difference organic surfactants as template and urea as hydrolysis adjusting agent (14). They studied the effects of cetyltrimethyl ammonium bromide, sodium dodecyl sulfate, and Triton X-100 on the morphology of NiO. NiO synthesized using sodium dodecyl sulfate exhibited a high specific capacitance of 235 F/g. Table 1.3 summarizes some of the electrochemical properties of nickel oxide.

Table 1.3: Specific capacitance values of NiO reported

Method	Substrate	Electrolyte	Measurement systems (condition)*	Specific capacitance (F/g)	(reference) year
Galvanostatic	Graphite	1 M KOH	CV (10 mV/s)	195	(15) 2006
SBA-15 as template	Ni grid	2 M KOH	CD (1 mA/cm^2)	128	(16) 2006
Porous hollow spheres of NiO	Glassy carbon electrode	2M KOH	CD (10 A/g)	560	(17) 2013
Hydrothermal (urea)	Ni foam	2M KOH	CD (200 mA/g)	138	(18) 2009
Via a Hydrothermal	Ni foam	2 M KOH	CV (3 mV/s)	989	(19) 2013
Hydrothermal (cetyltrimethyl ammonium bromide)	Ni foil	2 M KOH	CD (200 mA/g)	239	(14) 2010
Hydrothermal (sodium dodecyl sulfate)	Ni foil	2 M KOH	CD (200 mA/g)	411	(14) 2010
Hydrothermal (Triton X - 100)	Ni foil	2 M KOH	CD (200 mA/g)	144	(14) 2010
SDS as template and urea as hydrolysis Calcination at 1) 250 C 2) 300 C 3) 350 C	Ni Foam	3wt.% KOH	CD (200 mA/g)	1) 124 2) 106 3) 68	(20) 2004

* CV – cyclic voltammetry, CD – Galvanostatic charge-discharge

1.3: Dissertation Organization

This master's thesis has been divided into four chapters.

Chapter 1 is committed to the introduction of the topic and objectives for the present research. It additionally gives a short summary of different sorts of energy storage materials and their benefits.

Chapter 2 gives the method and experimental details about the synthesis of nickel oxide. Also, it presents a thorough hypothetical foundation for different techniques that can be utilized for the characterization of nickel oxide.

Chapter 3 contains the results and discussion of all experimental techniques. In addition, the results that we obtained through this research are compared with literature on nickel oxides.

Chapter 4 concludes with the results of the present research.

CHAPTER II

EXPERIMENTAL DETAILS

2.1: Materials and Synthesis

All the chemicals and solvents utilized in the experiments were of analytical grade and utilized without further purification. For the synthesis of nickel oxide having various morphologies, nickel (II) nitrate hexahydrate, urea CO $(NH_2)_2$, ammonium fluoride (NH_4F), cetyltrimethylammonium bromide (CTAB), poly (vinyl pyrrolidone) (PVP), sodium dodecyl sulfate (SDS) and DI water were used. The amount of reactants and solvents used in this work are given in Table 2.1.

Table 2.1: Experimental details for the synthesis of nickel oxide

Sample	$Ni(NO_3)_2.6HO$ (mg)	NH_4F (mg)	Urea (mg)	CTAB (mg)	PVP (mg)	SDS (mg)	DI Water (ml)
1	1450	400	1500	500	0	0	33
2	1450	400	1500	0	500	0	33
3	1450	400	1500	0	0	500	33

After mixing the reactants with help of bath sonication for 10 minutes, the mixed solution was then transferred into a 45 ml Teflon stainless steel autoclave. Then a piece of nickel foam, which was pre-cleaned and weighed, was immersed into the reaction solution and heated at 120° C for 10 h. The nickel foam was cleaned in 3 M HCl solution for 15 min using bath sonication to remove any surface oxides followed by cleaning in DI water, isopropanol and acetone. After drying, it was weighed. After 10 h of reaction at 120° C, the autoclave reactor was cooled down to room temperature naturally. The piece of nickel foam and the residue were washed several times with distilled water and absolute ethanol in order to remove the debris and residual reactant. After that, the sample which was synthesized using CTAB was heated at 350 ^{o}C for 3 h. The sample changes its color from light brown to green. The X-ray diffraction patterns were recorded and it was found that the sample was a mixture of NiO and Ni $(OH)_2$. The product was further heated 500 ^{o}C for 3 h. The color of the sample changed to brown after calcination at 500 ^{o}C. The X-ray diffraction study confirms the formation of phase pure NiO under this condition. Some researchers suggest that mixed phase of NiO provide a high charge storage capacity. To confirm this, the electrochemical testing of both the samples (calcine at 350 ^{o}C and 500 ^{o}C) was performed. It was observed that phase pure NiO provided high specific capacitance compared to mixed phases of NiO and Ni $(OH)_2$. The details of the x-ray diffraction patterns and electrochemical testing are given in the Results and Discussion section. Based on the electrochemical results, all the synthesized materials were calcined at 500° C for 3 h to completely convert the precursor to NiO phase.

2.2: Characterizations

The synthesized nickel oxide was characterized using various techniques such as X-ray diffraction, scanning electron microscopy and electrochemical analysis.

2.2.1: X-Ray Diffraction Study

X-ray diffraction is comprised of three fundamental elements: an X-ray tube, a sample holder, and an X-ray detector. The idea of X-ray diffraction depends on producing electrons by heating a filament in an X-ray electrode tube for creating an X-ray. Applying voltage to those electrons would accelerate the motion of electrons toward a sample. The structure of the synthesized nickel oxide was investigated utilizing a Shimadzu X-ray diffractometer utilizing the 2θ-θ scan with CuKα1 (λ=1. 5406 Å) radiation. 0.2 mm slits were utilized for the exporter and sensor sides. The X-ray was generated utilizing a high voltage of 40 kV and a current of 30 mA. The diffraction patterns were recorded while changing the incident angles between 10-80°. An X-ray sensor was put at a point that achieved the geometrical placement so that the angle between the atomic planes and the detector will be 2θ as shown in Figure 2.1.

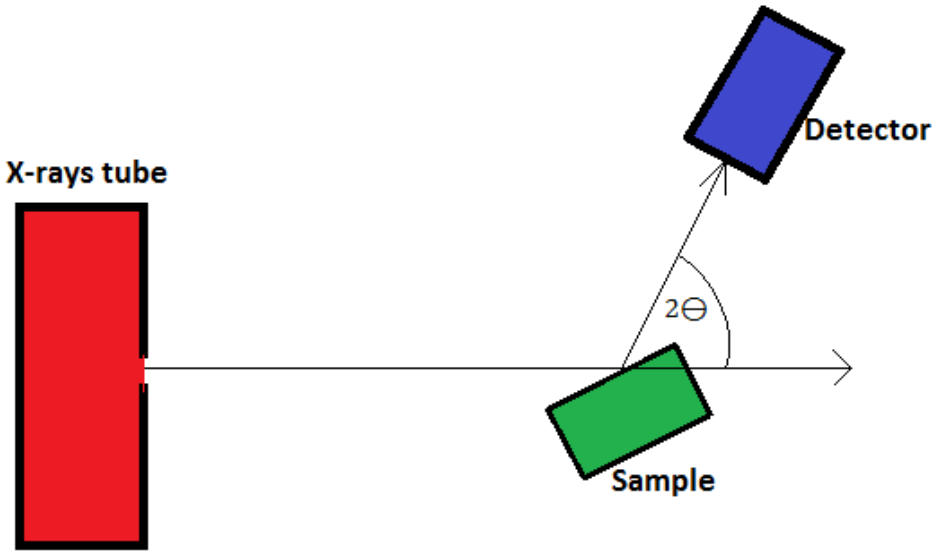

Figure 2.1: Schematic diagram of an X-ray diffractometer.

2.2.2: Scanning Electron Microscopy

In 1937 true microscopy was created by Manfred von Ardenne. In the 1960s, the first scanning electron microscopy (SEM) instrument appeared on the market. The scanning electron microscope is a valuable instrument that produces a picture of a sample when scanned by concentrated radiation of electron at its surface. The range of electron microscopes allows observation and also characterization of the materials around a nanometer (nm) to micrometer (μm).

The molecule extent and morphological placement of nickel oxide powder were examined utilizing a JEOL JSM-840A examining electron magnifying instrument as well as a FEI Quanta 200 field outflow examining electron microscopy (FESEM) prepared with an 16 oxford inca 250 silicon float X-beam vitality dispersive spectrometer (EDS).

2.2.3: Electrochemical Measurements

For electrochemical measurements of nickel oxides, a standard three electrode system containing a platinum wire as a counter electrode, saturated calomel electrode as a reference electrode, and NiO on nickel foam as a working electrode were used. The working electrode was prepared utilizing the synthesized NiO powder by blending 80 wt. % of the nickel oxide, 10 wt. % of acetylene black, and 10 wt. % of polyvinylidenedifluoride (PVDF) in N-methyl pyrrolidone (NMP) solvent. Then after blending the components, the obtained slurry was pasted onto nickel foam. The slurry pasted nickel electrodes were dried at 60° C under vacuum overnight. Three different alkaline solutions such as 3 M KOH, NaOH and LiOH were used as electrolytes for this study.

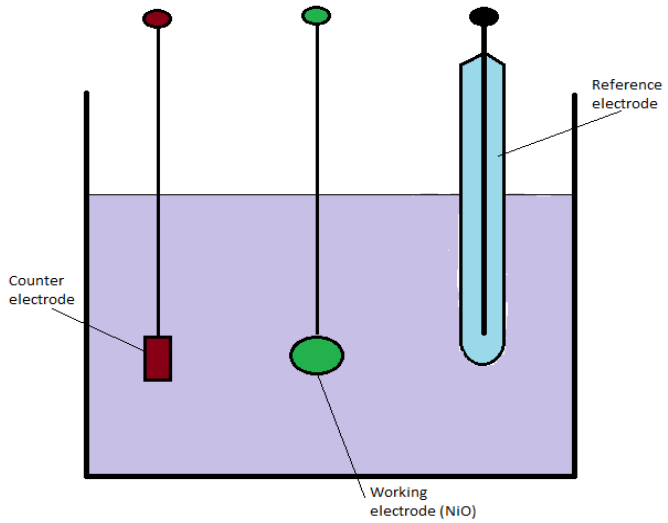

Figure 2.2: Schematic of three-cell electrochemical measurement system.

2.2.3.1: Cyclic Voltammetry

The electrochemical properties of the fabricated electrodes were studied using cyclic voltammetry. The cyclic voltammetry technique is used to potentially shift and monitor the resulting current by applying either positive or negative voltage under a constant scan rate. The current response was measured between the working and counter electrodes while potential was applied between the reference and working electrodes. When a positive potential was applied to the metal oxide, the following oxidation reaction occurred. The oxidized metal oxides reduce in the reverse cycles.

$$M \leftrightarrow M^{+} + e^{-}$$

2.2.3.2: Galvanostatic Charge – Discharge Measurements

Galvanostatic charge - discharge is a technique to measure the charge storage capacity and cycle life of electrode materials. The active mass of the NiO was calculated by the following equation:

$$\text{Active mass (g)} = \text{Total weight of the electrode materials (g)} \times 80\%$$

All the electrochemical measurements were performed using a Versastat 4-500 electrochemical instrument (Princeton Applied Research, USA). All the electrochemical data collected were analyzed using Versa Studio software from Princeton Applied Research. Before each measurement, the electrodes were activated by recording fifty cycles of cyclic voltammetric measurements in potential window of 0-0.6V at 50 mV/s of scan rate. After the warm up, cyclic voltammetric measurements were performed at

various scan rates (for CV curves) and current densities (for galvanostatic charge-discharge study).

CHAPTER III

RESULTS AND DISCUSSION

3.1: Optimizing Calcination Temperature

The as-synthesized sample was first calcined at 350 ^{o}C in air to study its phase purity and electrochemical properties. Calcination at 350 ^{o}C in air changed the color of as-synthesized powder from light brown to green. The X-ray diffraction patterns confirms the presence of two phases namely NiO and $Ni(OH)_2$. The X-ray diffraction pattern of the sample calcine at provided 350 ^{o}C is given in Figure 3.1. The calcination temperature was increased to 500 ^{o}C to see the effect of temperature on its phase purity. Figure 3.2 shows XRD pattern of brown sample which was obtained after calcination at 500 ^{o}C. As seen in the X-ray diffraction pattern, all the peaks were due to NiO and no other phases were found. The obtained peaks were well matched with the standard peaks of nickel oxide rock salt structure (diffraction peaks data of JCPDS no. 04-0835). This confirms the transformation of $Ni(OH)_2$ to NiO at 500 ^{o}C.

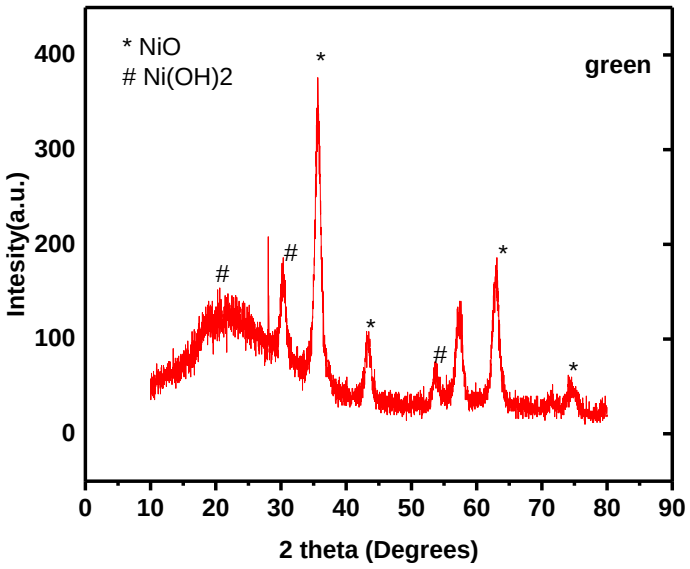

Figure 3.1: XRD pattern of green sample synthesized using CTAB at 350 °C.

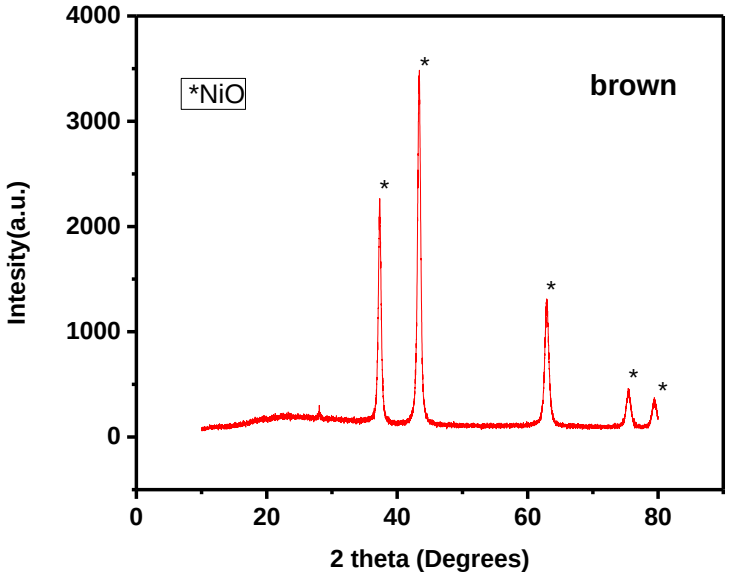

Figure 3.2: XRD pattern of NiO synthesized using CTAB at 500 °C.

In addition to X-ray diffraction study of the samples calcine at 350 ^{o}C and 500 ^{o}C, the electrochemical study was also performed using cyclic voltammetry and galvanostatic charge-discharge measurements. Figures 3.3 and 3.4 show the cyclic voltammograms of the samples calcine at 350 ^{o}C and 500 ^{o}C. As seen in the cyclic voltammogram, both the samples were redox active and provided oxidation and reduction peaks.

Figure 3.5 shows the variation of specific capacitance as a function of scan rates `for the samples calcine at 350 ^{o}C (mixed phases of $Ni(OH)_2$ and NiO) and 500 ^{o}C (phase pure NiO). As seen, the phase pure NiO which was obtained after calcining at 500 ^{o}C showed a higher specific capacitance than that of sample calcine at 350 ^{o}C. For example, the specific capacitance of samples calcine at 350 ^{o}C and 500 ^{o}C was observed to be 98 and 48 F/g at scan rate of 5 mV/s. Similar results were observed using galvanostatic charge-discharge study. Figure 3.6 shows the variation of specific capacitance as a function of applied current density for the both samples. The green powder which is related to $Ni(OH)_2$ and NiO showed a specific capacitance of about 25 F/g at a discharge current of 0.5 mA. In contrast, the brown powder which is phase pure NiO showed a specific capacitance of about 62 F/g at a discharge current of 0.5 mA. In conclusion, the phase pure NiO showed better electrochemical performance compared with mixed phases of NiO and $Ni(OH)_2$.

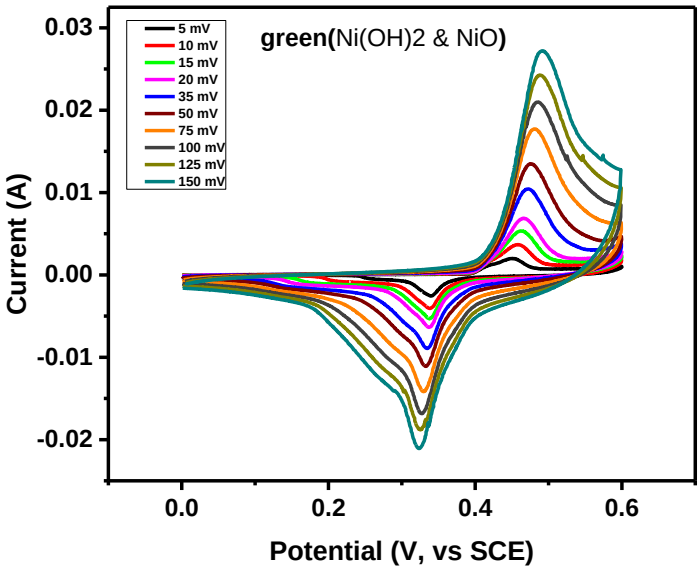

Figure 3.3: Cyclic voltammograms of NiO and Ni $(OH)_2$ synthesized using CTAB at 350 °C.

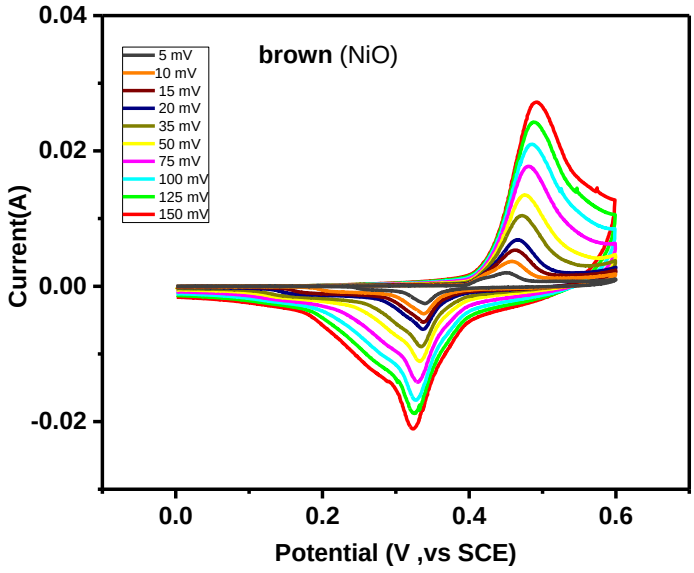

Figure 3.4: Cyclic voltammograms of NiO synthesized using CTAB at 500 °C.

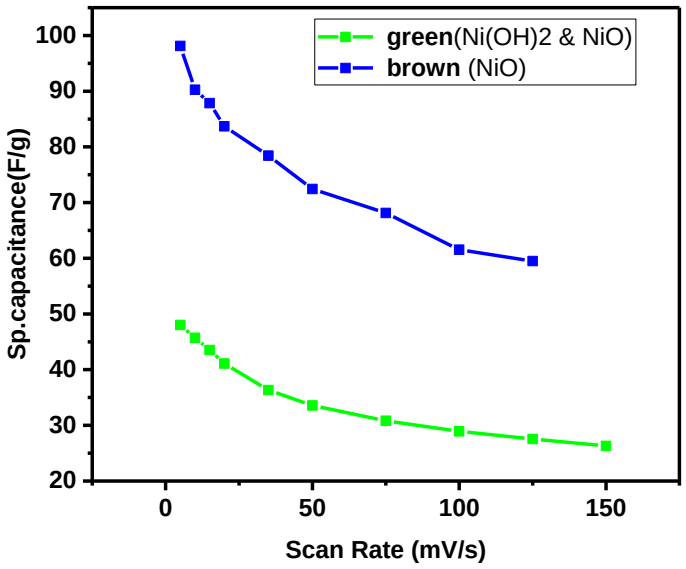

Figure 3.5: Variation of specific capacitance as a function of scan rate for nickel compounds synthesized using CTAB and calcined at difference temperatures.

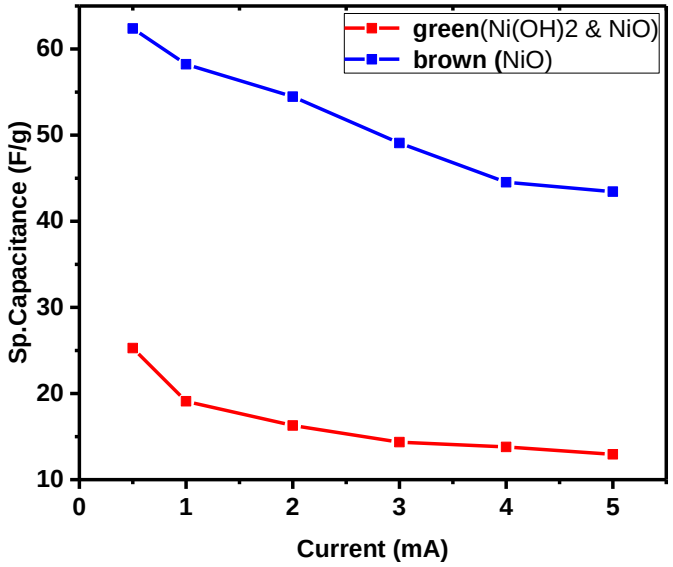

Figure 3.6: Variation of specific capacitance with applied current for nickel compounds synthesized using CTAB and calcined at difference temperatures.

3.2: X-Ray Diffraction Analysis

X-ray diffraction was used to examine the phase purity of the synthesized materials. Figures 3.7-3.9 show the XRD patterns of all the synthesized samples which were calcined at 500 ^{o}C. As seen in the XRD patterns, all the synthesized powders showed diffraction peaks. Three strong diffraction peaks were observed around 37, 43, and 63^{o} which matches well with the standard peaks of nickel oxide rock salt structure (diffraction peaks data of JCPDS no. 04-0835). The XRD patterns did not indicate any peaks other than peaks due to NiO. This confirms the absence of any other phases of nickel compound such as $Ni(OH)_2$, Ni_2O_2 etc. During the calcination at 500 ^{o}C in air, the following reaction occurred (20)

$$Ni(OH)_2 \rightarrow NiO + H_2O$$

Purushothaman et al. have also studied the effect of preparation temperature on the morphological and electrochemical properties on -assembled NiO microstructures (19). The peak of NiO in XRD patterns became sharper when synthesis temperature was increased from 120 °C to 180 °C. The temperature of heating might have been to decrease the electrochemical properties of nickel oxide. They reported that an optimum temperature in the range of 25° to 400° C was the best temperature to get high capacitance and high electrochemical activities (21, 22). Srinivasan and Weidner studied the effect of heating temperature on the charge storage capacity nickel oxide films (22). At about 300 °C, the specific capacitance sharpily increases to a value of 104 F/g and drops as the temperature increased.

The crystal size of the nickel oxide powders was estimated using X-ray data of the respective samples. The crystal size was estimated using the Debye Scherrer equation (23):

$$t=\frac{0.9\,\lambda}{\beta\cos\theta} \quad \text{.....(4),}$$

where 0.9 is assuming of the shape coefficient for reciprocal lattice, λ is the X-ray wavelength, β is the full width at half maximum of the diffraction line, and θ is the Bragg angle (the diffraction angle of the XRD spectra). Table 3.1 below shows the average crystalline size of our synthesized nickel oxides. Justin et al. obtained a smaller crystal size of about 2.25 nm when they synthesized NiO using anionic surfactant sodium dodecyl sulfate (14).

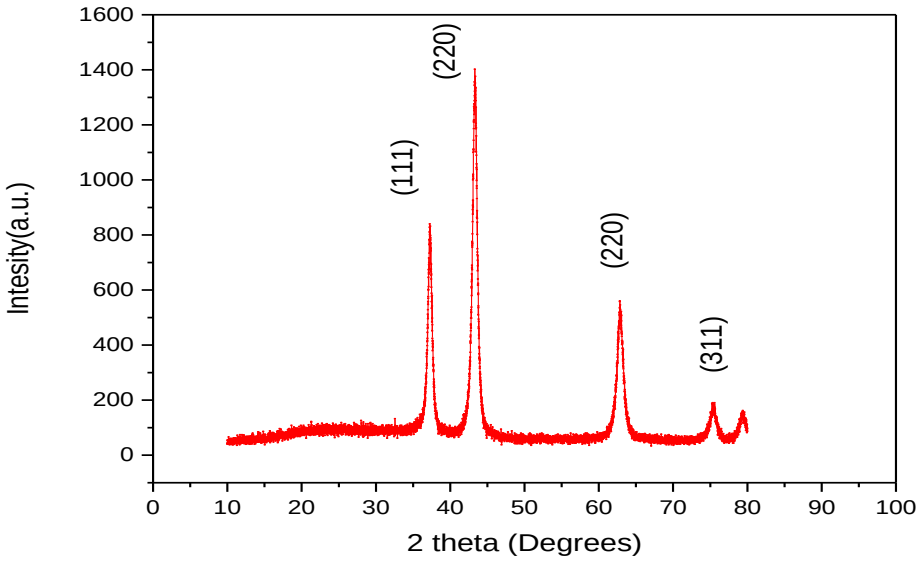

Figure 3.7: XRD patterns of NiO synthesized using CTAB.

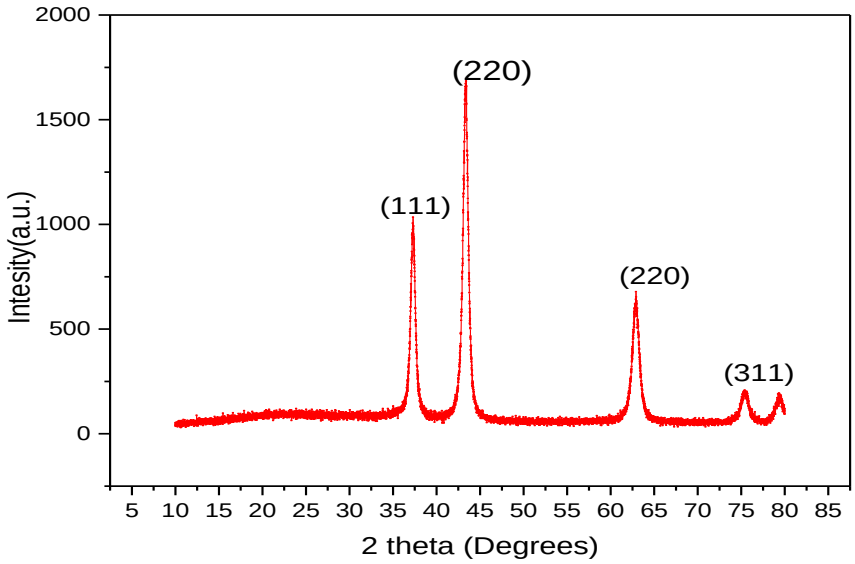

Figure 3.8: XRD pattern of NiO synthesized using PVP.

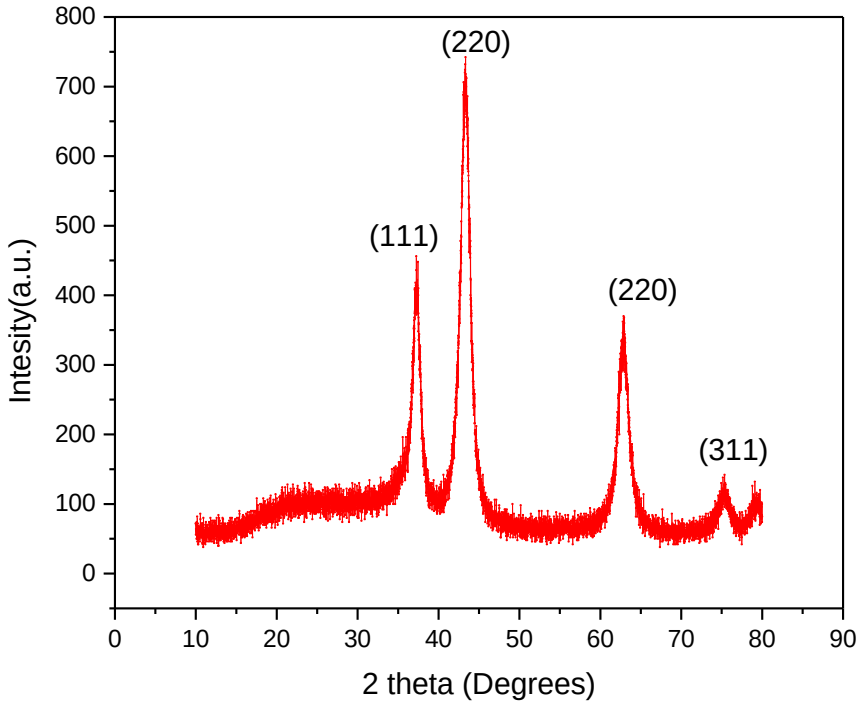

Figure3.9: XRD patterns of NiO synthesized using SDS.

Table 3.1: Crystalline size of the synthesized nickel oxide

Sample	FWHM (degree)	FWHM (Radian)	Crystallite Size(nm)
NiO-CTAB	0.75	0.013	18.2
NiO-SDS	1.33	0.023	27.5
NiO-PVP	0.72	0.013	16.3

The crystal size of nickel oxide was found to depend on the surfactant used during the reaction. It was observed that SDS provided nickel oxide with the highest crystal size of about 28 nm. On the other hand, PVP based nickel oxide provided the lowest crystal size of about 16 nm. Sheena et al have studied the effect of calcination temperature on the structural and optical properties of nickel oxide nanoparticles (24). They have synthesized nickel oxide using the chemical precipitation route. It was observed that when calcination temperature increased, the crystallite size also increased. It was further noted that the crystallinity of nickel oxide has a tremendous effect on their electrochemical properties. It is observed that synthesis method also affects the crystallite size of the nickel oxides. For example, Meybodi et al have synthesized NiO nano-powders using a sonochemical method and observed a crystallite size of about 20 nm (25).

3.3: Scanning Electron Microscopic Analysis

The surface morphology and structure of three nickel oxide samples were scrutinized by scanning electron microscopy.Figures 3.10 -3.12 show the scanning electron microscopy image of NiO synthesized using CTAB, SDS and PVP. The SEM

images gave us an idea about NiO structures that could explain the observed specific capacitance. It is known that the pore size affects the capacitance of electrodes,as reported by Liang and Han (26, 27). They have observed that the pore size in range of 2-5 nm was very appropriate to increase the capacitance of the nickel oxide.

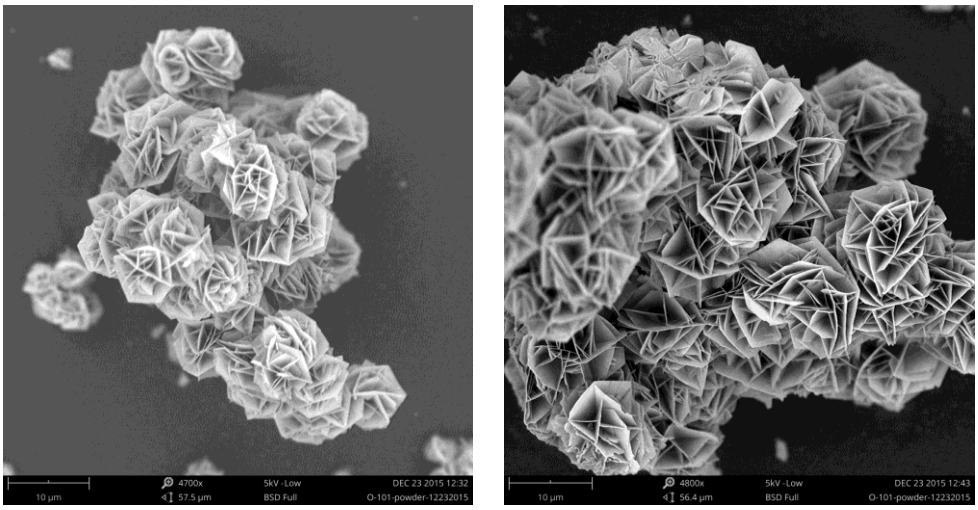

Figure 3.10a: SEM images of NiO powder sample synthesized using CTAP at various magnifications.

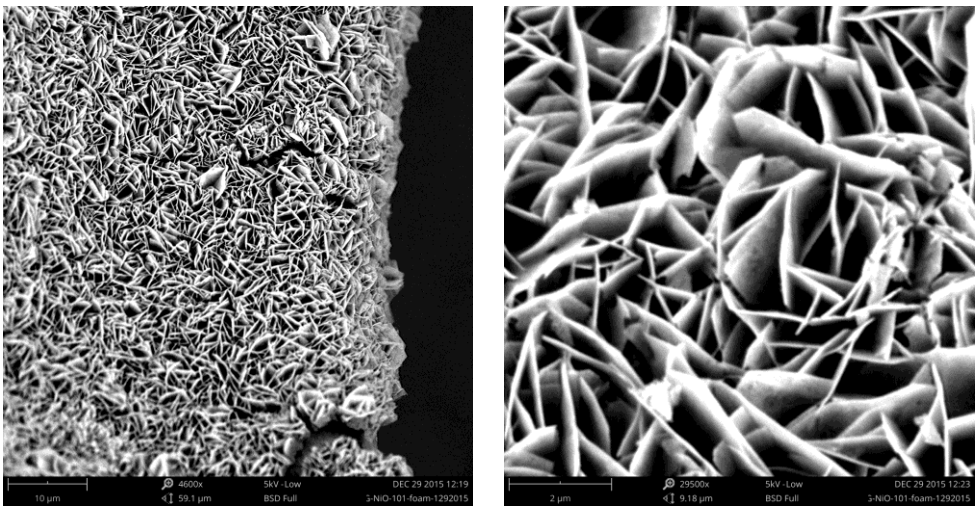

Figure 3.10b: SEM images of NiO on Ni foam synthesized using CTAP at various magnifications.

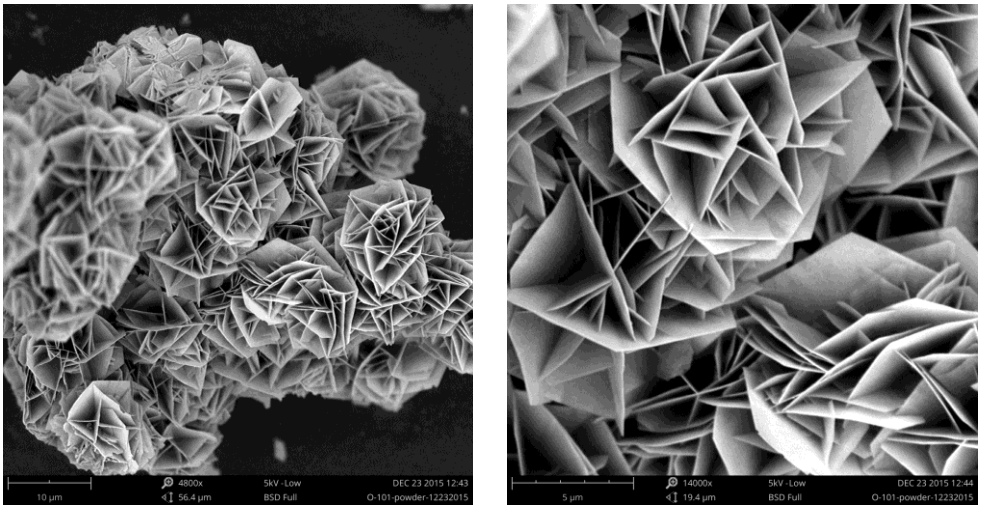

Figure 3.11a: SEM images of NiO powder sample synthesized using PVP at various magnifications.

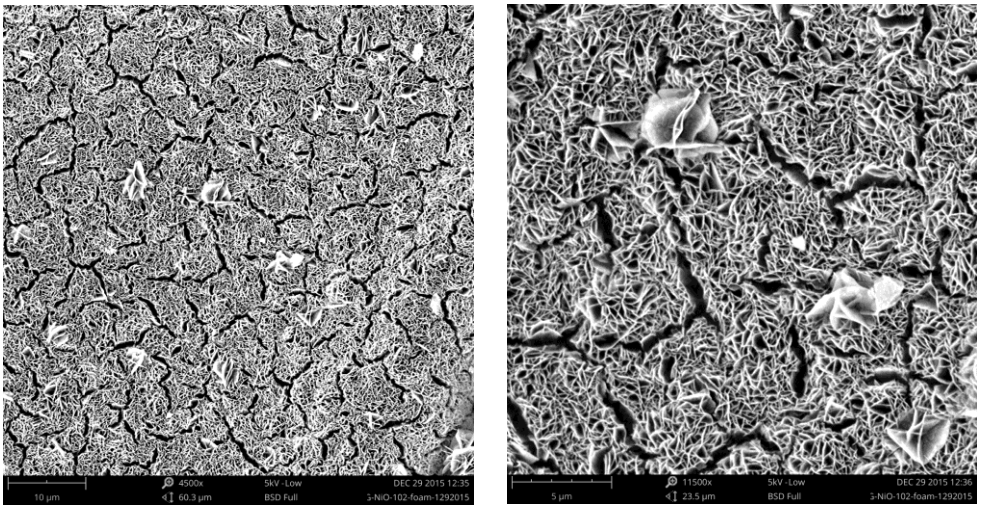

Figure 3.11b: SEM images of NiO on Ni foam synthesized using PVP at various magnifications.

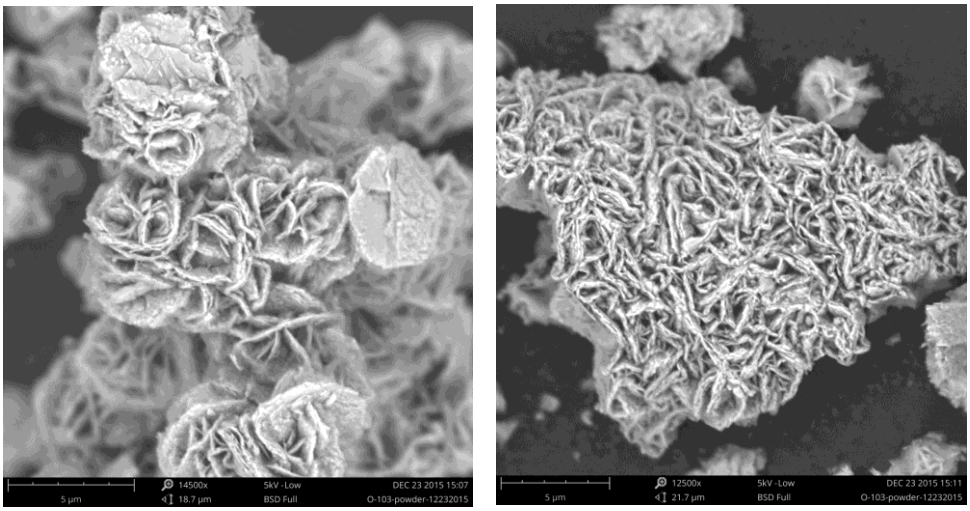

Figure 3.12a: SEM images of NiO powder sample synthesized using SDS at various magnifications

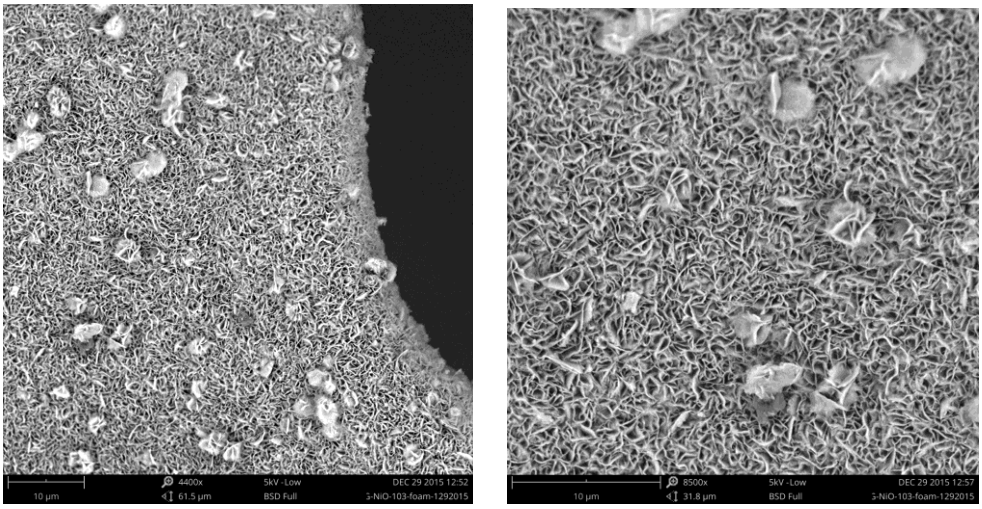

Figure 3.12b: SEM images of NiO on Ni foam synthesized using SDS at various magnifications.

3.4: Electrochemical Characterizations

The electrochemical properties of the NiO samples were examined using cyclic voltammetry and galvanostatic charge –discharge measurements. Three different electrolytes such as 3 M NaOH, KOH, and LiOH, were used to study the effect of ionic

size of the electrolytes on the electrochemical properties of the nickel oxides. Figures 3.13-3.24 show the cyclic voltammetry and the specific capacitance of the NiO at different scan rates. As seen in the cyclic voltammograms of nickel oxide, the shape of the CV curves is very similar even at higher scan rates suggesting high electrochemical stability of the nickel oxides. The process of redox reaction at the electrodes follows the reaction:

$$NiO + OH^- \leftrightarrow NiO\text{-}OH + e-$$

The specific capacitance of the nickel oxides was calculated using the CV data at various scan rates. The specific capacitance of nickel oxide was calculated using the expression given below (6):

$$C_{sp} = \frac{1}{mv(Vf-Vi)} \int_{Vi}^{Vf} i(V)dV \quad \text{.....(5),}$$

where C_{sp} is the specific capacitance (F/g), m is the mass of active material (g), v is the scan rate (V/s). V_i and V_f are the initial/final potential in volt of a CV cycle. $i(V)$ is the instantaneous current at a given potential. Figure 3.16 shows the variation of specific capacitance as a function of scan rates for a NiO sample synthesized using CTAB in different electrolytes. As seen in the graph, the specific capacitance of the nickel oxide was found to decreasing with increasing scan rates. The diminishing of capacitance could be explained by the presence of some interactive sites that cannot complete the redox reaction at the electrode because increasing scan rate led to decreasing the cyclic time. There are two main factors that can affect the amount of specific capacitance such as higher active area on the electrode and internal resistance. The conductivity will be decreased through increased scan rate because of increasing the internal charge–transfer resistance. The rate of redox reaction at the interface between the electrode surface and

the electrolyte is greatly affected and not kinetically favored. Such a conclusion can be attributed to the loss of some active material at the electrode surface during the experimental resulting in an incomplete redox reaction (26). In addition, the electrolytes can have an effect on specific capacitance. In Figure 3.16 the highest specific capacitance was calculated around 261.2 F/g for NiO synthesized using CTAB sample in 3M KOH electrolytes at scan rate 5 mV/s. The specific capacitance of NiO sample as shown in Figure 3.16 decreased to 226.5 F/g in NaOH electrolyte. The specific capacitance is further decreased to 223.3 F/g in the LiOH electrolyte. As observed the highest specific capacitance was observed in 3M KOH electrolytes. Figure 3.20 shows the specific capacitance of NiO synthesized using PVP. The highest specific capacitance value was observed when LiOH was used as the electrolyte. The highest specific capacitance of NiO-PVP sample was observed to be 163.4 F/g in 3M LiOH electrolyte. In contrast, the specific capacitance of 143 F/g was observed in 3M NaOH for the NiO-PVP sample. Figure 3.24 shows the variation of specific capacitance as a function of scan rates for a NiO synthesized using SDS in three different electrolytes. The specific capacitance values of 223.3, 226.5 and 261.2 F/g was observed for NiO synthesized using SDS in 3 M KOH, NaOH and LiOH electrolytes, respectively at a scan rate of 5 mV/s. The NiO synthesized using SDS showed the highest specific capacitance value in all electrolytes compared with other NiO samples. Justin et al. had reported a specific capacitance of 321 F/g for NiO synthesized using SDS at scan rate of 2 mV/s (14).

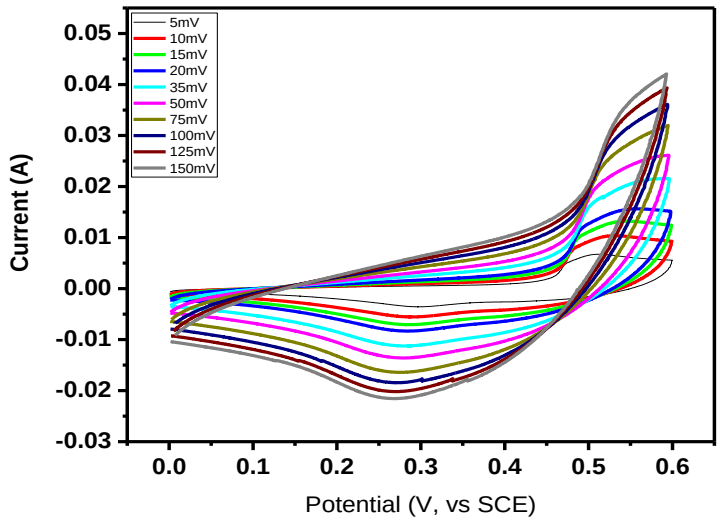

Figure 3.13: Cyclic voltammograms of NiO synthesized using CTAB at various scan rates in 3 M LiOH electrolyte.

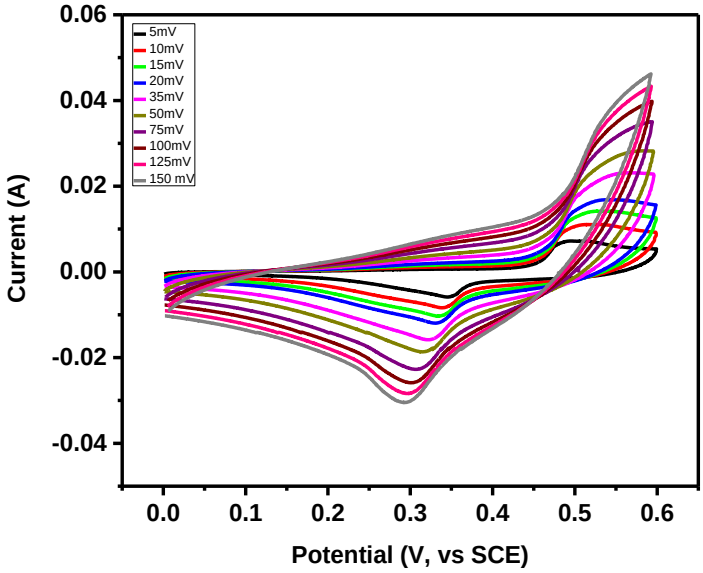

Figure 3.14: Cyclic voltammograms of NiO synthesized using CTAB at various scan rates in 3M NaOH electrolyte.

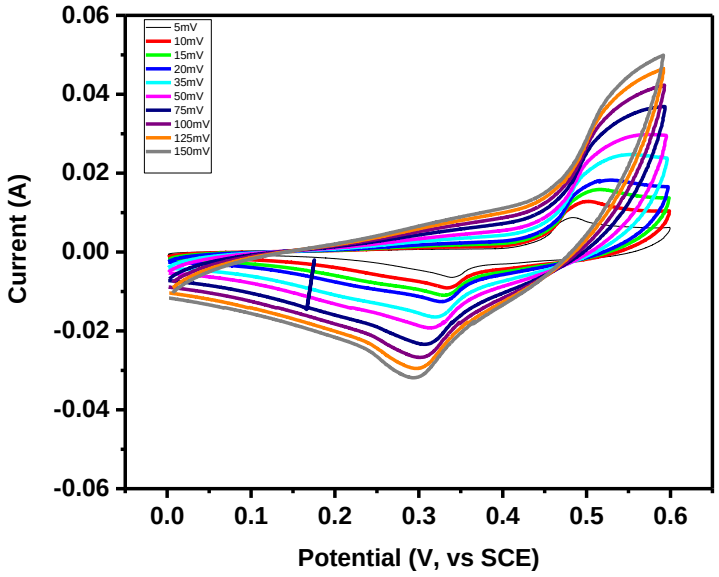

Figure 3.15: Cyclic voltammograms of NiO synthesized using CTAB at various scan rates in 3 M KOH electrolyte.

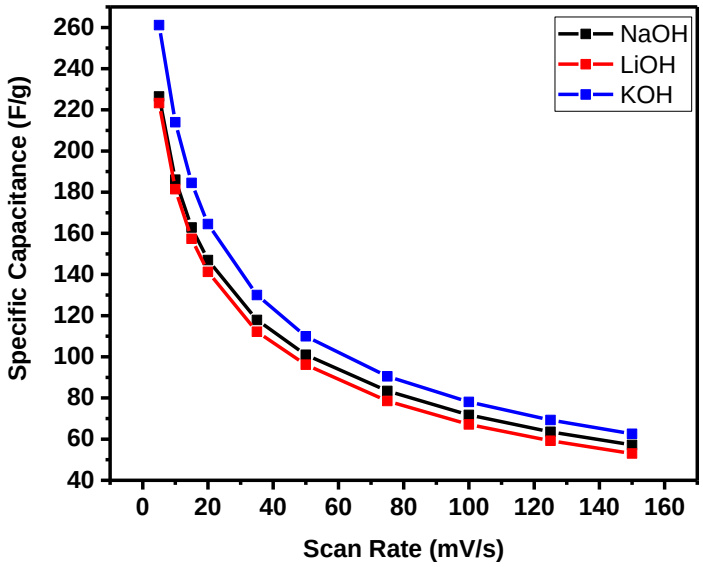

Figure 3.16: Variation of specific capacitance as a function of scan rate for NiO synthesized using CTAB sample in difference electrolytes.

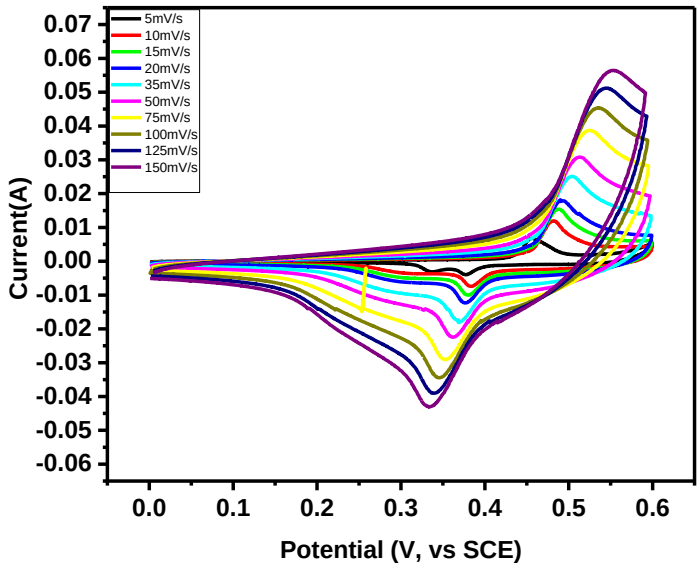

Figure 3.17: Cyclic voltammograms of NiO synthesized using PVP at various scan rates in 3 M LiOH electrolyte.

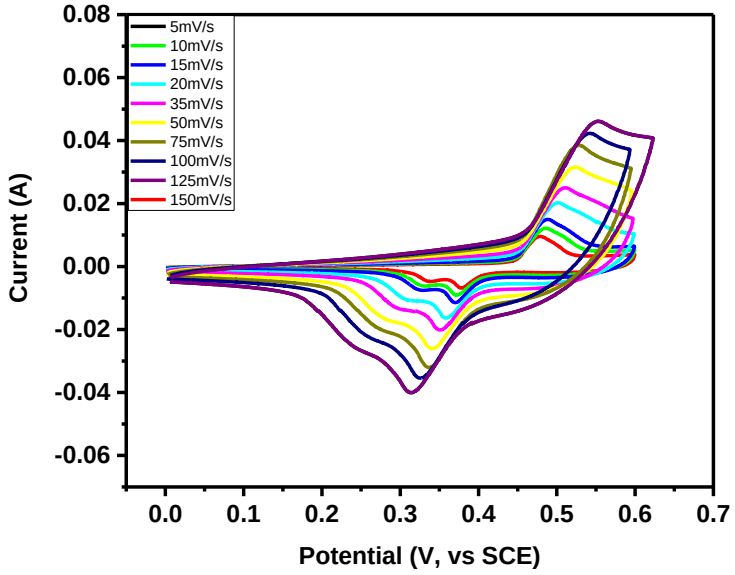

Figure 3.18: Cyclic voltammograms of NiO synthesized using PVP at various scan rates in 3 M NaOH electrolyte.

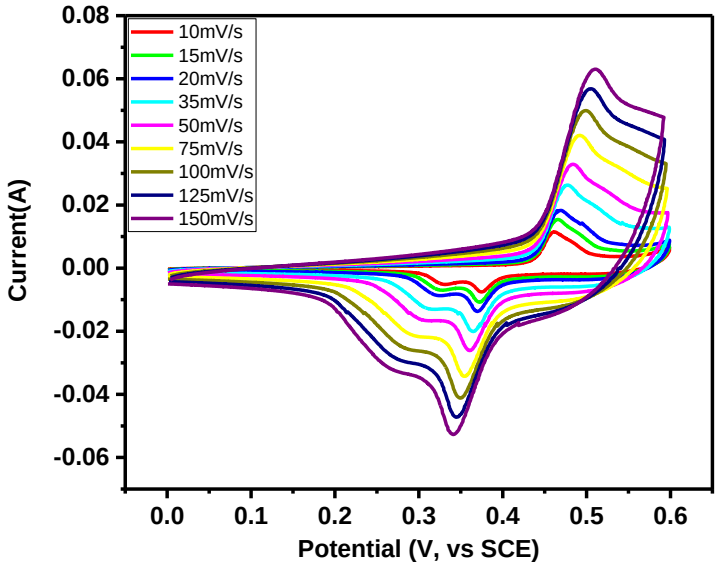

Figure 3.19: Cyclic voltammograms of NiO synthesized using PVP at various scan rates in 3 M KOH electrolyte.

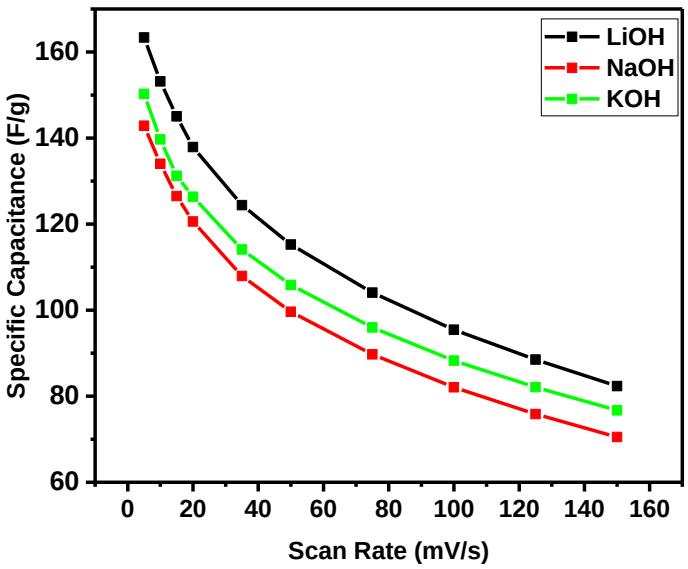

Figure 3.20: Variation of specific capacitance as a function of scan rate for NiO synthesized using PVP sample in difference electrolytes.

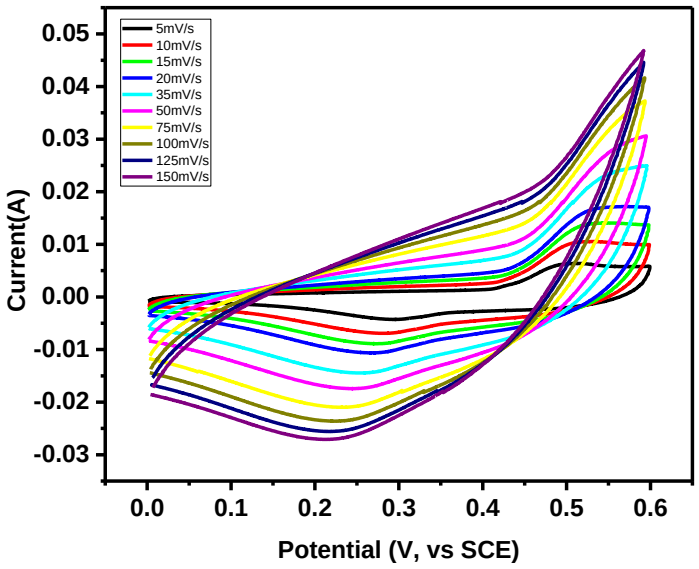

Figure 3.21: Cyclic voltammograms of NiO synthesized using SDS at various scan rates in 3 M LiOH electrolyte.

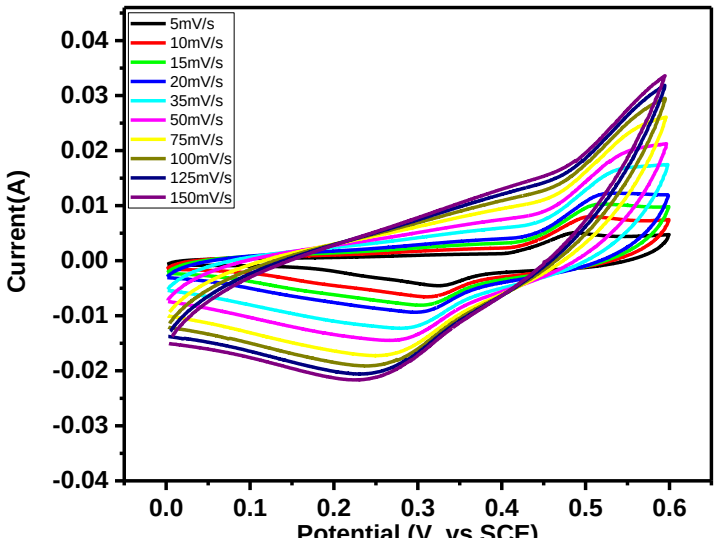

Figure 3.22: Cyclic voltammograms of NiO synthesized using SDS at various scan rates in 3 M NaOH electrolyte.

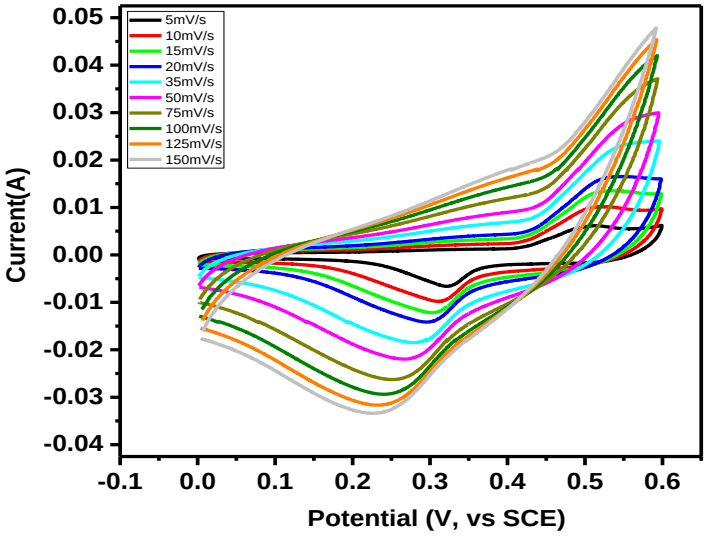

Figure 3.23: Cyclic voltammograms of NiO synthesized using SDS at various scan rates in 3 M KOH electrolyte.

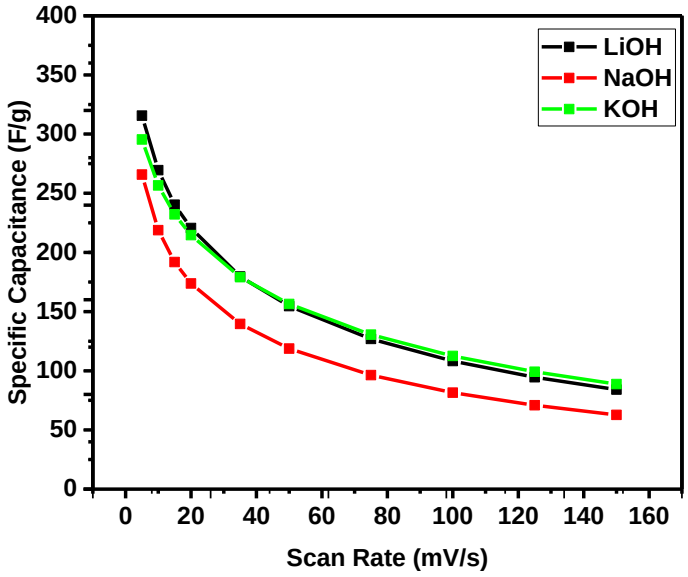

Figure 3.24: Variation of specific capacitance as a function of scan rate for NiO synthesized using SDS sample in difference electrolytes.

The specific capacitance of any material depends on the active sites which participate in the redox reaction. The usage factor of nickel oxide sites, which was participatory, in nickel oxide was calculated by the following equation (19):

$$Z = \frac{C\,M\Delta V}{F} \quad \text{.....(6),}$$

where C is the specific capacitance (F/g), M is the molecular weight (74.7 g/mol), ΔV is the potential window (V). The highest value of z is 1 which means that all the nickel oxide sites on an electrode has contributed to the redox/reduction reaction. Table 3.2 shows the part of the nickel oxide sites (z) that contributed to the redox reaction in NiO sample synthesized using CTAB in 3 M KOH electrolyte. The highest value of 12.1% was observed at scan rate of 5 mV/s. In contrast, when the scan rate was increased to 150 mV/s, the value of z dropped to 4. In Tables 3.3 and 3.4, z values of NiO were shown in 3M NaOH and LiOH electrolytes. It was seen that the z values decrease with increase in the scan rates.

Table 3.2: The percentage of fraction for nickel oxide sites, z which has been participatory in the redox reaction of NiO synthesized using CTAB in 3 M KOH electrolyte:

Scan Rate (mV)	Csp (F/g)	Z%
5	261.2	12.1
10	214.0	9.94
15	184.5	8.57
20	164.5	7.64
35	130.0	6.04
50	109.9	5.11
75	90.5	4.20
100	78.1	3.63
125	69.3	3.22
150	62.6	2.91

Table 3.3: The percentage of fraction for nickel oxide sites, z which has been participatory in the redox reaction of NiO synthesized using CTAB in 3 M NaOH electrolyte:

Scan Rate (mV)	Csp (F/g)	Z%
5	226.5	10.6
10	186.0	8.7
15	162.9	7.6
20	147.0	7.0
35	118.0	5.6
50	101.0	4.7
75	83.4	3.9
100	71.8	3.4
125	63.6	3.0
150	57.2	2.7

Table 3.4: The percentage of fraction for nickel oxide sites, z, which has been participatory in the redox reaction of NiO synthesized using CTAB in 3 M LiOH electrolyte:

Scan Rate (mV)	Csp (F/g)	Z%
5	223.3	10.4
10	181.4	8.5
15	157.3	7.4
20	141.2	6.6
35	112.2	5.3
50	96.2	4.5
75	78.6	3.7
100	67.2	3.1
125	59.2	2.7
150	53.0	2.5

Table 3.5: The percentage of fraction for nickel oxide sites, z, which has been participatory in the redox reaction of NiO synthesized using PVP in 3 M LiOH electrolyte:

Scan Rate (mV)	Csp (F/g)	Z%
5	163.4	7.6
10	153.2	7.1
15	145.0	6.8
20	138.0	6.4
35	124.4	5.8
50	115.3	5.4
75	104.1	5.0
100	95.5	4.5
125	88.6	4.12
150	82.4	4.0

Table 3.6: The percentage of fraction for nickel oxide sites, z which has been participatory in the redox reaction of NiO synthesized using PVP electrode in 3 M NaOH electrolyte:

Scan Rate (mV)	Csp (F/g)	Z%
5	143.0	6.6
10	134.0	6.2
15	126.6	5.9
20	120.6	5.6
35	107.9	5.0
50	99.6	4.7
75	89.7	4.2
100	82.1	3.9
125	75.9	3.6
150	70.6	3.3

Table 3.7: The percentage of fraction for nickel oxide sites, z which has been participatory in the redox reaction of NiO synthesized using PVP electrode in 3 M KOH electrolyte:

Scan Rate (mV)	Csp (F/g)	Z%
5	150.3	7.0
10	139.7	6.5
15	131.2	6.1
20	126.4	5.9
35	114.1	5.3
50	105.9	5.0
75	95.9	4.5
100	88.3	4.1
125	82.1	3.9
150	76.8	3.6

Tables 3. 6 and 3. 7, above, show the percentage of fraction of NiO synthesized using PVP sites, which has been contributed in redox reaction. The value of z in all three electrolytes is similar. Srinivasan and Weidner have been studied the effect of heating temperature and electrolyte concentration on the z sites of nickel oxide (22). It was suggested that a lower z value can be related to that redox reaction, which only occurred at the active surface of NiO with little dimensional interaction. Also, the size of OH^- can have an effect on the diffusion of OH^- into material. Table 3.6 shows the z value of scan rate 5 mV was 6.6% which was contributed in the redox reaction of NiO synthesized using PVP electrode in NaOH electrolyte to produce specific capacitance around 142.9 F/g.

Table 3.8: The percentage of fraction for nickel oxide sites, z which has been participatory in the redox reaction of NiO synthesized using SDS electrode in 3 M LiOH electrolyte:

Scan Rate (mV)	Csp (F/g)	Z%
5	315.6	14.7
10	269.5	12.5
15	240.3	11.2
20	220.6	10.2
35	179.7	8.3
50	154.618	7.2
75	126.9	6.0
100	108.2	5.0
125	94.5	4.4
150	84.1	4.0

Table 3.9: The percentage of fraction for nickel oxide sites, z which has been participatory in the redox reaction of NiO synthesized using SDS electrode in 3M NaOH electrolyte:

Scan Rate (mV)	Csp (F/g)	Z%
5	265.8	12.3
10	218.7	10.2
15	191.9	9.0
20	173.8	8.1
35	139.6	6.5
50	118.8	5.6
75	96.3	4.5
100	81.5	3.8
125	70.9	3.3
150	62.8	3.0

Table 3.10: The percentage of fraction for nickel oxide sites, z which has been participatory in the redox reaction of NiO synthesized using SDS electrode in 3M KOH electrolyte:

Scan Rate (mV)	Csp (F/g)	Z%
5	295.5	13.8
10	256.7	12.0
15	232.1	10.8
20	214.7	10.0
35	179.1	8.3
50	156.4	7.3
75	130.6	6.1
100	112.6	5.2
125	99.1	4.6
150	88.8	4.2

The highest value of z as seen in the Table 3.8 was 14.7%, and it was observed for the NiO synthesized using SDS. This z value means around 14.7 percent of nickel oxide sites had participated in redox reaction during the electrochemical testing process. So, this percentage explains why the NiO synthesized using SDS had the highest value of specific capacitance around 315.6 F/g in 3M LiOH electrolyte compared to other electrolytes. Moreover, this also explains the decrease in the specific capacitance with the increase in the scan rates. At higher scan rates, the z values are lower, suggesting less active sites were participating in the redox process. Vijayakumar et al. had prepared NiO nanomaterial using CTAB as surfactant via microwave synthesis method at various calcination temperatures (28). They observed a specific capacitance of about 400 F/g at calcination temperature of 300 ^{o}C with z value around 14%. When the calcination temperature was increased to 400 and 500 °C, value of z was calculated to be around 8.35 and 7.17%, respectively. So, in those samples only 8.5% and 7.17% of sites on the

electrode had participated in redox reaction to produce a specific capacitance 240 and 206 F/g. Table 3.9 shows the z value was 12.3 % of NiO synthesized using SDS when NaOH electrolyte was used. In this electrolyte the specific capacitance of NiO was 265.5 F/g which means only 12.3% site of NiO was contributed in reaction. Table 3.10 shows the z value of NiO synthesized using SDS in KOH electrolyte. The highest z value was 13.8% in Table 3.10 related to KOH electrolyte 5 mV which give us specific capacitance around 295.3 F/g.

In addition to a cyclic voltammetry study, galvanostatic charge-discharge measurements were performed to evaluate the potential application of nickel oxide as an electrode material for supercapacitor. The galvanostatic charge-discharge measurements were carried out in 3 M KOH, NaOH and LiOH. The charge-discharge tests were performed in potential range of 0 to 0.6 V (vs. SCE) at different current densities ranging from 1 mA /g to 5 mA/g. Figures 3.25-3.33 show the charge-discharge curves of NiO synthesized using CTAB, SDS and PVP samples. Figures 3.25-3.27 show the charge-discharge measurements of NiO synthesized using CTAB. The galvanostatic charge-discharge studies indicated that the highest discharge time of 109 s was observed at 0.5 mA/g in3 M KOH electrolyte, whereas the lowest discharge time of 87 s was observed at 0.5 mA/g in 3 M LiOH electrolyte. Figures 3.28-3.30 show the galvanostatic charge-discharge measurements of a NiO synthesized using PVP electrode. The electrode activities of galvanostatic charge-discharge performance at three electrolytes are almost equivalent with little change in discharge time. The longest discharge time of 83.8 s was received in 3 M KOH electrolyte. Figures 3.31- 3.33 show the galvanostatic charge-discharge behaviors of the NiO synthesized using SDS in different electrolytes. The NiO

showed a discharge time of 156 s at 0.5 mA/g in 3 M LiOH, which was the longest discharge time compared to that of in other NiO samples. Figure 3.33 shows that the lowest discharge time was observed for the NiO synthesized using SDS in 3 M NaOH electrolyte at a current density of 0.5 mA/g. Xing Wei et al have reported that there are two factors which can have an effect on the capacitance of a NiO electrode, surface area and surface reactivity (20).The specific capacitance of the nickel oxide electrodes was computed utilizing the following equation (13):

$$\mathbf{C_s}= \frac{I\times\Delta t}{\Delta V\times m} \quad \text{.....(7),}$$

where C_s is the specific capacitance (F/g), I is the charge /discharge current (A), Δt is the discharge time(s), m is the mass of electrode material (g), and ΔV is the discharging potential range (V). Figures 3.34-3.3.36 show the relationship between the specific capacitance and current. As we see in the specific capacitance equation above, the specific capacitance will be increased with increased discharge current but this does not occur. This is due to a large voltage drop at higher discharge currents which lead to a decrease in specific capacitance (27). The OH^- anion will be received or released during the oxidation –reduction process and the exchange of OH^- occurred between the electrolyte and the electrode at the interface. When the reduction reaction occurs, the OH^- anion is transferred to the electrode by diffusion. Also, when the oxidation reaction happens the OH^- anion should be retained back to the electrolyte. The optimal electrochemical performance occurs when the OH^- and electron are transported at the same time or in synchronization together. The OH^- has a slower transfer process than the electron transport. So, at higher discharge currents, the OH^- ion could not synchronize with the electron transfer due to the fact that the electron has high mobility. As a

consequence, the OH^- gets oversaturated which makes some of the surface area on the electrode inactive (17). Thereby, the highest specific capacitance was received at a current of 0.5 mA. In contrast, the lowest specific capacitance was observed at a current of 5 mA. Gobal and Faraji have reported that at higher charge-discharge levels, only the outer layers contribute to the redox process (29). As seen in Figure 3.36, the highest specific capacitance of 130 F/g was observed for NiO synthesized using SDS in 3 M LiOH electrolyte. Liu et al. have synthesized urchinlike NiO nanostructures and studied their electrochemical behaviors (30). They observed that calcination temperature affects the charge storage capacity e.g. calcination temperature of 300 and 500 °C provided specific capacitance of 290 and 170 F/g, respectively.

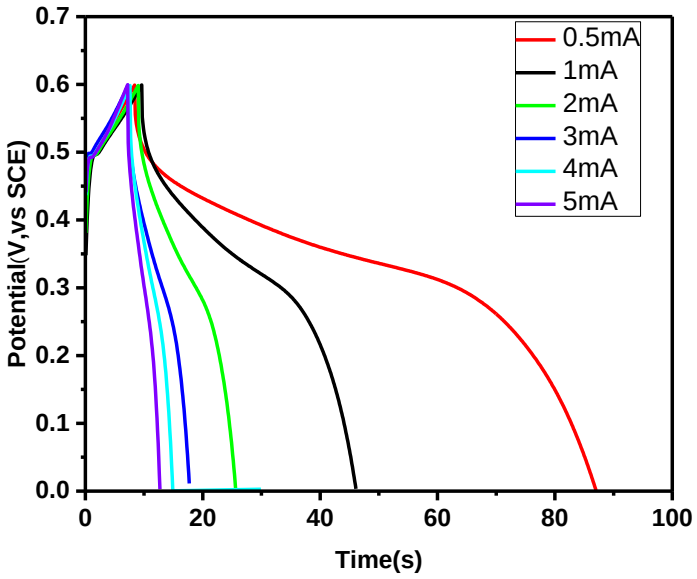

Figure 3.25: Galvanostatic charge –discharge characteristics of NiO synthesized using CTAB at various currents in 3 M LiOH electrolyte.

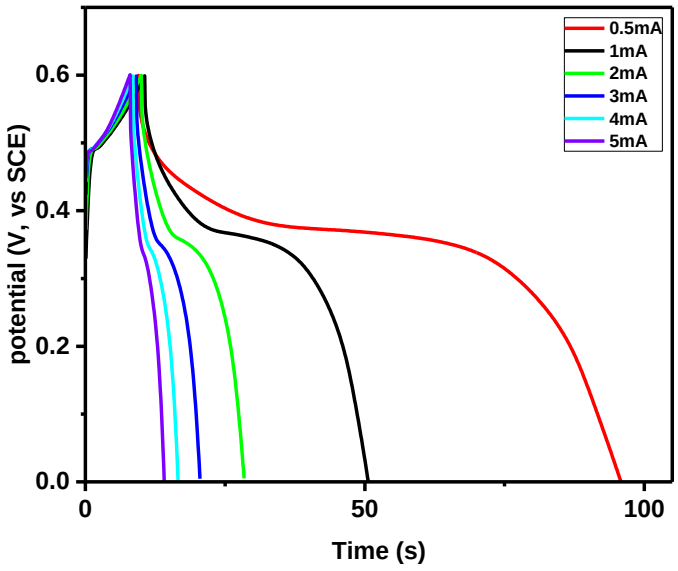

Figure 3.26: Galvanostatic charge–discharge characteristics of NiO synthesized using CTAB at various currents in 3 M NaOH electrolyte.

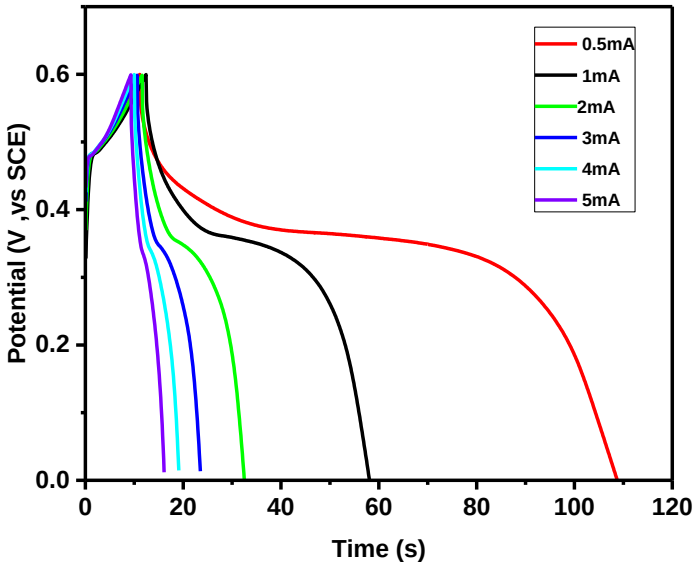

Figure3.27: Galvanostatic charge –discharge characteristics of NiO synthesized using CTAB at various currents in 3 M KOH electrolyte.

Figures 3.25-3.27 show the charge–discharge behaviors of NiO synthesized using CTAB at various currents such as 0.5, 1, 2, 3, 4, and 5 mA in 3 M LiOH, NaOH and KOH. Figure 3.25 shows that the lowest discharge time was observed for the NiO synthesized using CTAB in 3M LiOH electrolyte. Figure 3.27 shows the galvanostatic charge –discharge measurements of NiO synthesized using CTAB in KOH electrolyte. The discharge times at 0.5 mA was around 109 s, which is the highest among other electrolytes. Figure 3.26 shows the galvanostatic charge – discharge measurements of NiO synthesized using CTAB in 3M NaOH electrolyte. The discharge times at 0.5 mA was around 98 s.

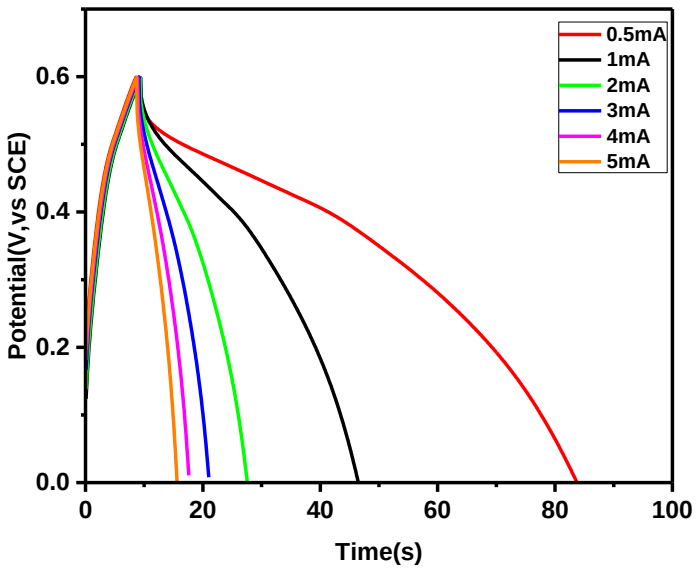

Figure 3.28: Galvanostatic charge –discharge characteristics of NiO synthesized using PVP at various currents in 3 M LiOH electrolyte.

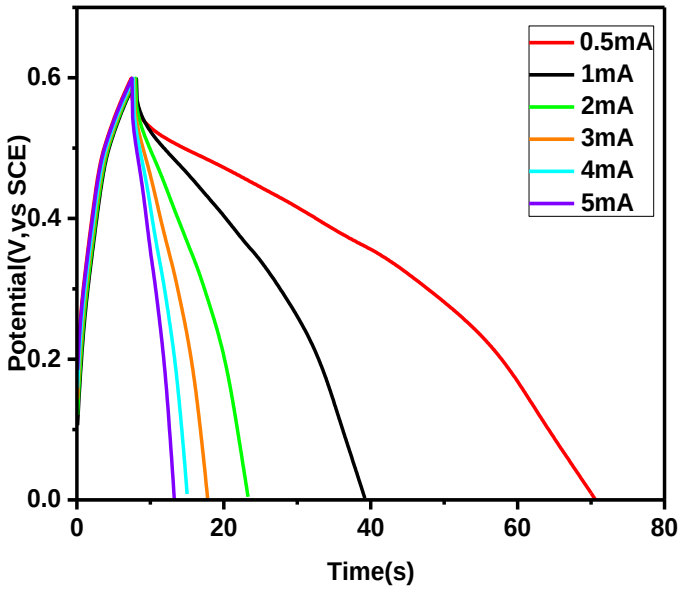

Figure 3.29: Galvanostatic charge –discharge characteristics of NiO synthesized using PVP at various currents in 3 M NaOH electrolyte.

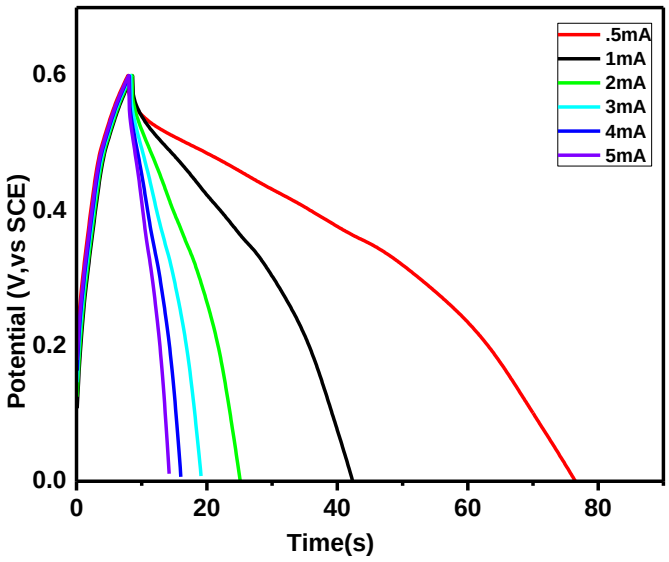

Figure 3.30: Galvanostatic charge –discharge characteristics of NiO synthesized using PVP at various currents in 3 M KOH electrolyte.

Figures 3.28-3.30 show the charge–discharge behaviors of NiO synthesized using PVP at various currents in 3 M LiOH, NaOH and KOH. As seen in Figure 3.28, the discharge time of 84 s was observed at discharge current of 0.5 mA in LiOH electrolyte. This was the highest discharge time observed for NiO synthesized using PVP. Figure 3.30 shows the galvanostatic charge –discharge of NiO synthesized using PVP in KOH electrolyte. The discharge times at 0.5 mA was about 76.5 s. Figure 3.28 shows the charge-discharge behavior of NiO in 3 M NaOH electrolyte.

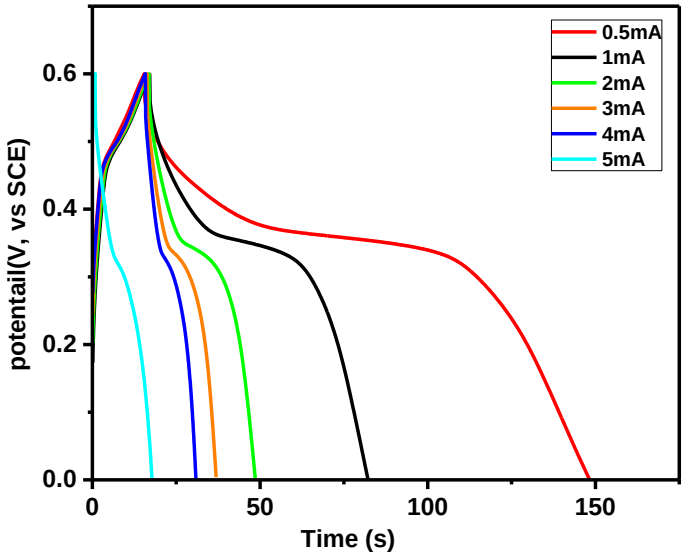

Figure 3.31: Galvanostatic charge –discharge characteristics of NiO synthesized using SDS at various currents in 3 M KOH electrolyte.

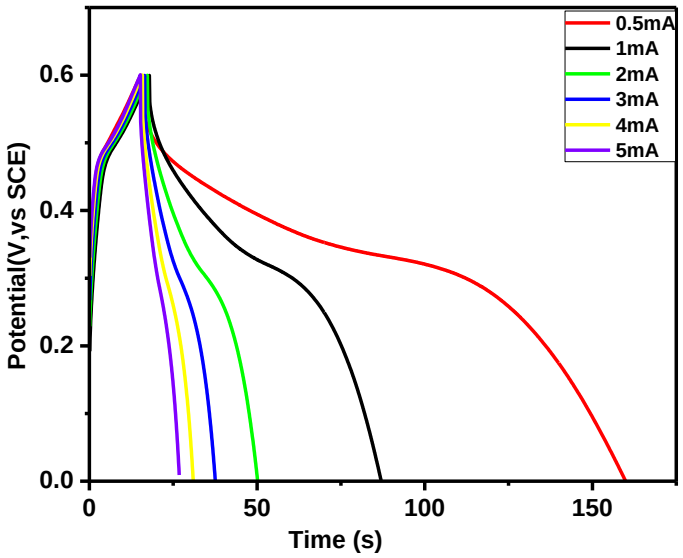

Figure 3.32: Galvanostatic charge –discharge characteristics of NiO synthesized using SDS at various currents in 3 M LiOH electrolyte.

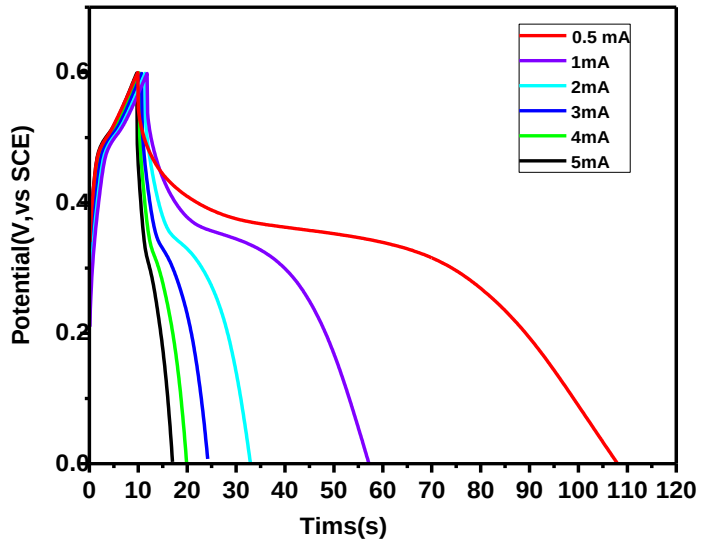

Figure 3.33: Galvanostatic charge –discharge characteristics of NiO synthesized using SDS at various currents in 3 M NaOH electrolyte.

Figures 3.31-3.333 show the charge–discharge behaviors of NiO synthesized using SDS at different discharge currents in 3 M LiOH, NaOH and KOH. A discharge

time of 148 s was observed at a discharge current of 0.5 mA in 3M KOH electrolyte. Figure 3.32 shows the galvanostatic charge –discharge behavior of NiO synthesized using SDS in LiOH electrolyte. The NiO synthesized using SDS showed the longest discharge time at 0.5 mA in LiOH. The discharge times at 0.5 mA was observed to be around 160s. Figure 3.33 shows the charge-discharge behavior of NiO behavior in NaOH electrolyte.

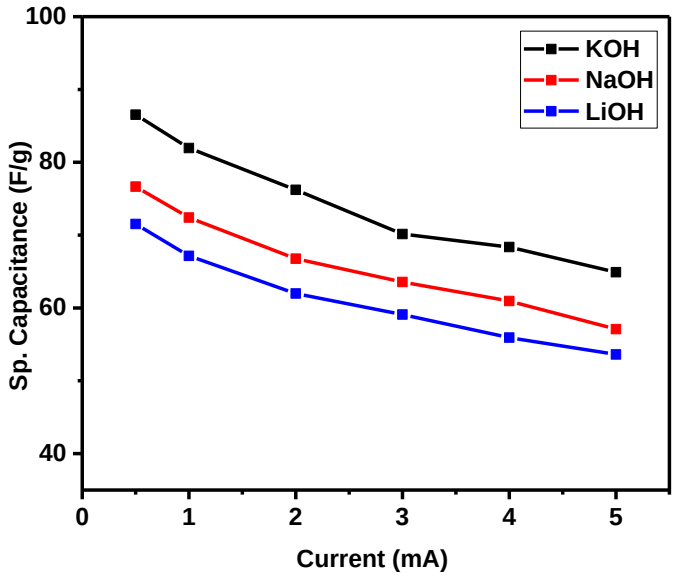

Figure3.34: Variation of specific capacitance with applied current in different electrolytes for NiO synthesized using CTAB.

Figure 3.34 shows variation of specific capacitance with applied current in different electrolytes for the NiO synthesized using CTAB. The highest specific capacitance of 86.6 F/g was observed in KOH electrolyte, while the lowest specific capacitance of NiO synthesis using CTAB was observed to be 72 F/g in LiOH electrolyte. The specific capacitance of about 77 F/g was observed in NaOH electrolyte.

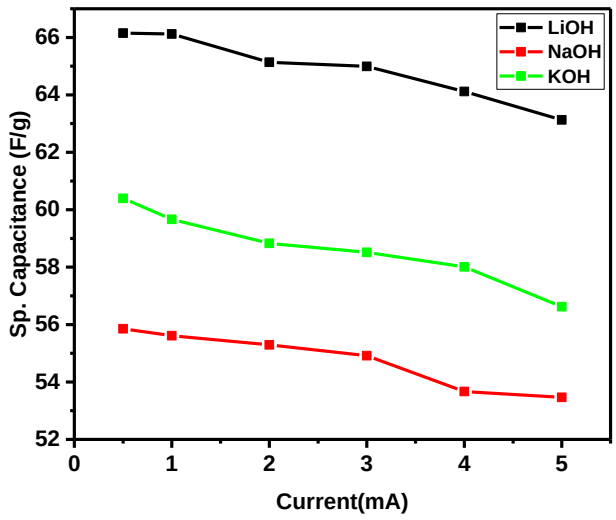

Figure3.35: Variation of specific capacitance with applied current in different electrolytes for NiO synthesized using PVP sample.

The specific capacitance of NiO synthesized using PVP is shown in Figure 3.35. A specific capacitance of 66 F/g was observed in LiOH electrolyte. The specific capacitance decreases to 56 F/g in KOH electrolyte. The specific capacitance of NiO synthesized using SDS was 63 F/g at current density 5 mA. All the samples have shown a decrease in specific capacitance with increase in the current density. Figure 3.36 shows the variation of specific capacitance as a function of applied current in different electrolytes for NiO synthesized using SDS. Unlike the results in Figures 3.34 and 3.35, the specific capacitance of NiO synthesized using SDS showed the highest specific capacitance value around 130 F/g in LiOH electrolyte. Also, in the LiOH electrolyte the specific capacitance of NiO synthesized using SDS at a current density 5 mA was about 115 F/g. The NiO synthesized using SDS showed the different performance in KOH electrolyte. The specific capacitance of NiO in KOH electrolyte at current density 0.5 mA was 118 F/g. Unlike the result in LiOH and KOH electrolytes of NiO synthesized using

SDS the specific capacitance shows the lowest electrochemical performance of NiO synthesized using SDS when NaOH electrolyte is used. The specific capacitance in NaOH electrolyte for NiO synthesized using SDS of 95 F/g at a current density of 0.5 mA. In addition, Figure 3.35 shows that the specific capacitances of all three samples are decreased with increased current densities.

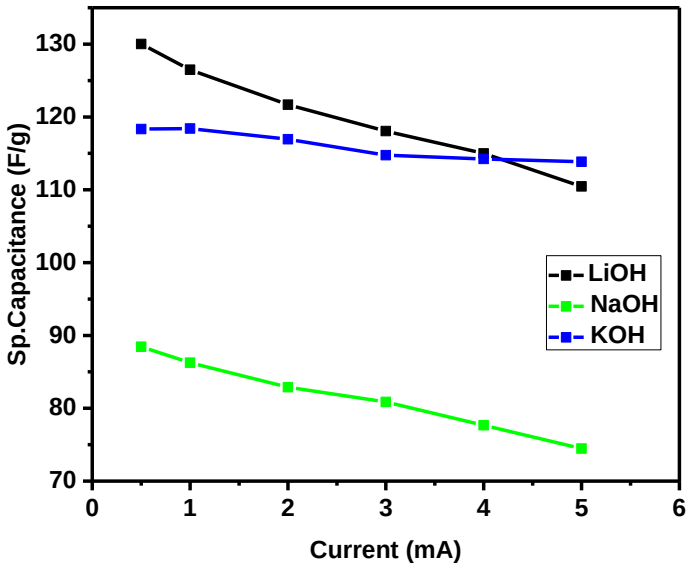

Figure3.36: Variation of specific capacitance with applied current in different electrolytes for NiO synthesized using SDS.

Power density and specific energy was used to evaluate the performance of nickel oxide. The Ragone plot showed the relationship between energy density and power density of samples which resulted from the charge –discharge measurements. Both energy density and power density were calculated by the following equation (31):

$$E\ (Wh/Kg) = \frac{Csp \times \Delta V \mathbf{2}}{7.2} \quad \text{.....(8)}$$

$$P\ (w/kg) = \frac{E \times 3600}{t} \quad \text{.....(9),}$$

where C_{sp} (F/g) is the specific capacitance that was calculated from charge –discharge measurements, ΔV (V) is the potential window and t(s) is the discharge time. Figures 3.37 -3.39 show the power density versus energy density plots for all the samples. At the lower discharge currents, the higher energy density was observed. In three samples the highest power density was obtained when 3 M LiOH electrolytes was used. In addition, NiO synthesized using SDS showed the highest power density. When the discharge current was increased the energy density was decreased, while the power density was increased. Kun Liang et al. have observed a high energy and power densities around 170 Wh/g and 27.5 kW/g, respectively in the potential window of 1.1 V (26). Purushothaman et al. have synthesized nanosheet – assembled NiO microstructure using a hydrothermal method at different temperatures (19). The NiO sample prepared at 160 °C presented a high energy density around 49.5 Wh/kg.

Figure 3.37 shows the variation of power density versus energy density for NiO synthesized using CTAB in different electrolytes. An energy density of 3.8 Wh/kg was observed in 3M KOH electrolyte. The energy density of 3.1 and 3.3 Wh/kg was calculated for the same sample in 3M LiOH and NaOH, respectively.

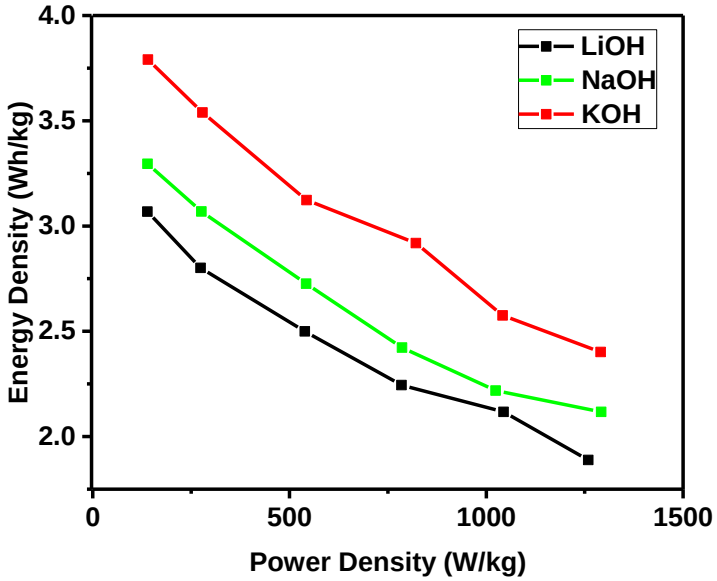

Figure 3.37: Power density versus energy density plots for NiO synthesized using CTAB in different electrolytes.

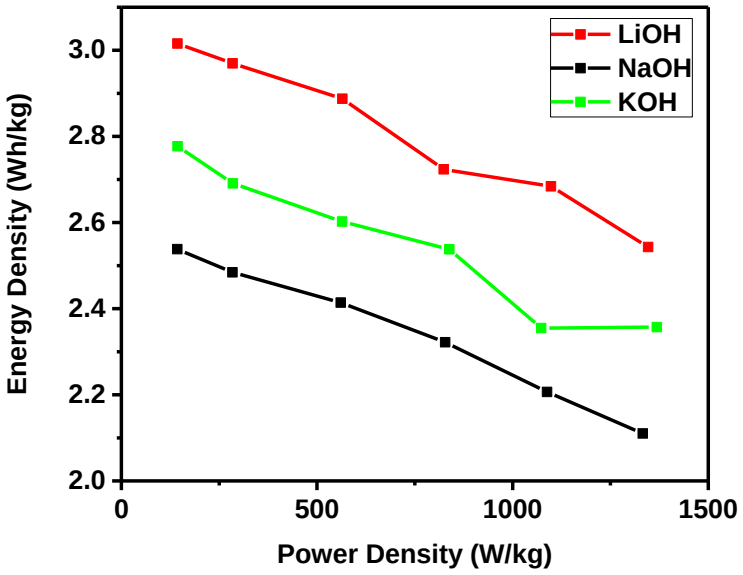

Figure 3.38: Power density versus energy density plots for NiO synthesized using PVP in different electrolytes.

Figure 3.38 shows the power density versus energy density for NiO synthesized using PVP in different electrolytes. At a power density of 143.2 W/kg, there was an energy density of 3 Wh/kg in LiOH electrolyte. As seen, in NaOH electrolyte the NiO showed the lowest value of energy density (~ 2.5 Wh/kg).

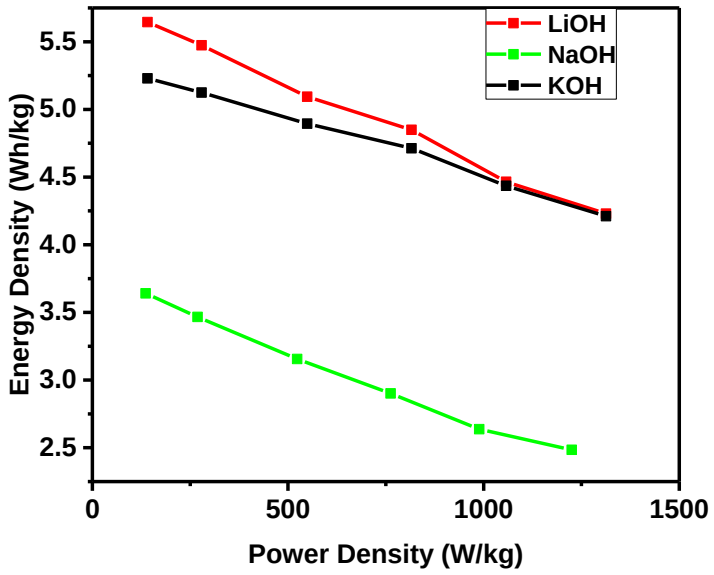

Figure 3.39: Power density versus energy density plots for NiO synthesized using SDS in different electrolytes.

Figure 3.39 show the variation of power and energy densities for NiO synthesized using SDS in different. Unlike the result in Figures 3.37 and 3.38, the energy density showed the highest value. An energy density of 5.6 Wh/kg was observed in LiOH electrolyte which decreased to 3.6 Wh/kg in NaOH electrolyte.

CHAPTER IV

CONCLUSION

Nickel oxide was synthesized using a hydrothermal technique. During hydrothermal reaction, the nickel precursor converted to nickel hydroxide which completely transformed into nickel oxide during calcination at 500 °C. It was seen that the presence of surfactants during reaction changes the morphology and sizes of nickel oxide. These synthesized nickel oxides were structurally and electrochemically characterized. Structural characterization was performed using X-ray diffraction and scanning electron microscopy. Electrochemical properties of nickel oxide were investigated using cyclic voltammetry and galvanostatic charge-discharge methods. The XRD pattern of the synthesized nickel oxide powders showed a clear phase of nickel oxide without any impurity phases. The crystalline size of nickel oxide was calculated using XRD data. It was observed that crystal size depends on the surfactants. Crystal size of 27, 19 and 16 nm was observed for nickel oxides when SDS, CTAB and PVP were used, respectively. The scanning electron microscopy images showed that surfactant also changes the morphology of nickel oxide. It was observed that these variations affect the electrochemical behavior of nickel oxides. All the electrochemical measurements were done using a standard three-electrode cell in a potential range of 0 to 0.6 V. Redox peaks

were observed in the cyclic voltammetry study of these samples. The specific capacitance was observed to decrease with increase in scan rate. It was further observed that specific capacitance depends on the electrolyte used. In addition, the morphological structure of nickel oxide also affects its specific capacitance. The highest specific capacitance is 315 F/g which was observed in 3 M LiOH for NiO-SDS at scan rate 5 mV/s. The percentage of electroactive sites (z) on the nickel oxide electrode which participated in redox reaction was calculated. The z value of nickel oxide was calculated from specific capacitance as the function of scan rate and 12.1, 7.5 and 14.6% was observed for NiO-CTAB, NiO-PVP and NiO-SDS, respectively at 5 mV/s. NiO-SDS gives the highest percentage of z, suggesting that about 14.6% of the electroactive sites participated in the redox reaction which gave the highest specific capacitance. The galvanostatic charge – discharge tests were further used to study the electrochemical properties of nickel oxide. The galvanostatic charge –discharge behavior showed that specific capacitance depends on discharge current and electrolyte used. When the current density was increased, the specific capacitance of nickel oxide was observed to decrease. The maximum specific capacitance of 130 F/g was observed in 3 M LiOH electrolyte for NiO-SDS sample. The power and energy densities were also calculated for all the nickel oxide samples. Both power and energy densities were depending on the electrolytes and current densities. The high power density was observed in 3 M LiOH electrolyte for NiO-SDS sample.

REFERENCES

1. J. Figueiredo and M. Guillén, Green Power: Perspectives on sustainable electricity generation. CRC Press, Feb 5, 2014.
2. Office of energy efficiency & renewable energy. http://energy.goc/eere/office-energy-efficiency-renewable-energy (accessed Mar 8, 2016).
3. P. Du and N. Lu, Renewable electricity sources energy storage for smart grids: planning and operation for renewable and variable energy resources (VERs). Academic Press, Oct 18, 2014.
4. S. Kalogirous, Solar Energy Engineering: Processes and systems. Elsevier/Academic press: Burlington, MA, 2009.
5. T. B. Buchner, N. H. Ewingen, Photosynthesis: Theory and applications in energy, biotechnology and nanotechnology. Nova Science Publishers: New York, 2009
6. Solar cells - the three generations .http://plasticphotovoltaics.org/lc/lc-solarcells/lc-introduction.html (accessed Jan 13, 2016).
7. E. Alqurashi, Facile Synthesis and electrochemical analysis of cobalt sulfide nanostructures for supercapacitor. MS Thesis, Pittsburg State University, Pittsburg, Kansas, 2015.
8. M. Lu and F. Beguin and E. Frackowiak, Supercapacitors: Materials, systems, and applications. Wiley VCH: Weinheim, 2013.
9. B. Ding, and J. Yu, Electrospun Nanofibers for Energy and environmental applications. Springer Berlin-Verlag Heidelberg, 2014.
10. K. Kumar, G. Kumar and A. Verma, Super capacitor. International Journal of Innovative Research in Technology, 1(2014) 2349.

11. K. Raj, V. Thangaraj and A.P. Uthirakumar, Synthetic routes to nickel oxide nanoparticles- an overview. Chemical Science Review and Letters, 4 (2015) 494.
12. K. Liu, and M. Anderson, Porous nickel oxide/nickel films for electrochemical capacitors. J. Electrochem. Soc, 143 (1996) 124.
13. D. Leontyeva, I. Leontyev, M. Avramenko, Y. Yuzyuk, Y. Kukushkina and N. Smirnova, Electrochemical dispergation as a simple and effective technique toward preparation of NiO based nanocomposite for supercapacitor application. Electrochimica Acta, 114 (2013) 356.
14. P. Justin, S. -K. Meher and G. -R. Rao, Tuning Of capacitance behavior of NiO using anionic, cationic, and nonionic surfactants by hydrothermal synthesis. Journal of Physical Chemistry, 114 (2010) 5203.
15. M. Wu, J. Gao, S. Zhang and A. Chen, Comparative studies of nickel oxide films on different Substrates for electrochemical supercapacitors. Journal of Power Sources, 159 (2006) 365.
16. Y.-G. Wang and Y.-Y. Xia, Electrochemical capacitance characterization of NiO with ordered mesoporous structure synthesized by template SBA-15. Electrochemical Acta, 51 (2006) 3223.
17. W.Yu, X. Jiang, S. Ding, B. Q. Li, Preparation and electrochemical characteristics of porous hollow spheres of NiO nanosheets as electrodes of supercapacitors. Journal of Power Sources, 256 (2014) 440.
18. Y.-Z. Zheng, H.-Y. Ding and M.-L. Zhang, Preparation and electrochemical properties of nickel oxide as a supercapacitor electrode material. Materials Research Bulletin, 44 (2009) 403.

19. K. K. Purushothaman, I. M. Babu, B. Sethuraman and G. Muralidharan, Nanosheet-Assembled NiO Microstructures for high-performance supercapacitors. ACS Applied Materials & Interfaces, 2013, 5 (21), 10767–10773.
20. W. Xing, F. Li, Z.-F. Yan and G. Lu, Synthesis and electrochemical properties of mesoporous nickel oxide. Journal of Power Sources, 134 (2004) 324.
21. M.-S. Wu, Y.-R. Zheng and G.-W. Lin, Three-dimensional carbon nanotube networks with a supported nickel oxide nanonet for high-performance supercapacitors. Chemical Communication Chem, 50 (2014) 8246.
22. V. Srinivasan, and J. W. Weidner, Studies on the capacitance of nickel oxide films: effect of heating temperature and electrolyte concentration. Journal of the Electrochemical Society J. Electrochem. Soc, 147 (2000) 880.
23. S. A. Studenikin, N. Golego and M. Cocivera, Fabrication of green and orange photoluminescent, undoped ZnO films using spray pyrolysis. Journal of Applied Physics, 84 (1998) 2287.
24. P. Sheena, K. Priyanka, N. Sabu, B. Sabu and T. Varghese, Effect of calcination temperature on the structural and optical properties of nickel oxide nanoparticles. Nanosystem: Physics, Chemistry, Mathematics, 5 (2014) 441.
25. S. M. Meybodi, S. Hosseini, M. Rezaee, S. Sadrnezhaad and D. Mohammadyani, Synthesis of wide band gap nanocrystalline NiO powder via a sonochemical method. Ultrasonics Sonochemistry, 19 (2012) 841.
26. K. Liang, X. Tang, B. Wei and W. Hu, Fabrication and characterization of a nonporous NiO film with high specific energy and power via an electrochemical dealloying approach. Materials Research Bulletin, 48 (2013) 3829.

27. D. Han, P. Xu, X. Jing, J. Wang, D. Song, J. Liu and M. Zhang, Facile Approach to Prepare Hollow Core–shell NiO microspheres for supercapacitor electrodes. Journal of Solid State Chemistry, 203 (2013) 60.
28. S. Vijayakumar, S. Nagamuthu and G. Muralidharan, Supercapacitor studies on NiO nanoflakes synthesized through a microwave route. ACS Appl. Mater. Interfaces ACS Applied Materials & Interfaces, 5 (2013) 2188.
29. F. Gobal and M. Faraji, Fabrication of nonporous nickel oxide by de-zincification of Zn–Ni/ (TiO_2-nanotubes) for use in electrochemical supercapacitors. Electrochimica Acta, 100 (2013) 133.
30. X.-M. Liu, X.-G. Zhang and S.-Y. Fu, Preparation of urchinlike NiO nanostructures and their electrochemical capacitive behaviors. Materials Research Bulletin, 41 (2006) 620.
31. C. Xiang, M. Li, M. Zhi, A. Manivannan and N. Wu. A reduced graphene oxide/Co_3O_4 composite for supercapacitor electrode. J. Power Sources, 226 (2013) 65.